Technische Universität Wien

Fakultät für Elektrotechnik und Informationstechnik

DIPLOMARBEIT

Investigation on Distance Measurement with Chirped Laser Light

ausgeführt zum Zwecke der Erlangung des akademischen Grades eines Diplom-Ingenieurs am

Institute of Electrodynamics, Microwave and Circuit Engineering

unter der Leitung von

Univ.Prof. Dr. Horst Zimmermann
Dr. Robert Swoboda

durch

B.Sc. Matthias F. Brandl
Mat. Nr. 0226080
Reisenbauer-Ring 1/1/12
2351 Wr. Neudorf

Wien, Juni 2010

Matthias Brandl

Vienna University of Technology

Faculty of Electrical Engineering and
Information Technology

Diploma Thesis

Investigation on Distance Measurement with Chirped Laser Light

Institute: Institute of Electrodynamics,
Microwave and Circuit Engineering

Supervisors: Univ.Prof. Dr. Horst Zimmermann
Dr. Robert Swoboda

Author: B.Sc. Matthias F. Brandl
Mat. Nr. 0226080
Reisenbauer-Ring 1/1/12
2351 Wr. Neudorf

Vienna, June 2010

Matthias Brandl

Abstract

In this thesis, interferometric distance measurements with chirped laser light from a frequency-shifted feedback laser are demonstrated. With this method, the length measurement process is converted into a frequency measurement process. Compared to other length measurement principles such as triangulation or time-of-flight measurement, interferometric methods usually have a better length resolution. With the full optical bandwidth, a length resolution of 0.2mm was achieved. Thereby each peak in the radio-frequency spectrum was resolved with only one test frequency. If a more time- and hardware-consuming measurement process were used, in which each peak is resolved with several test frequencies, the length resolution would be improved even further. Since this principle provides a high length resolution for small-area electronic circuits, it is an ideal candidate to build a sensor array for a three-dimensional camera.

Contents

List of Figures

List of Tables

1 Introduction

The development of three-dimensional (3D) cameras emerges rapidly because the field of possible applications of such cameras increases significantly. The field ranges from low-cost systems for gaming consoles to person tracking systems in public places, or to high accuracy systems with detailed 3D models for scientific purposes.
The three basic methods to do distance measurement are triangulation, time-of-flight measurement and interferometric measurement. In triangulation, the light source and the camera have known positions and the distance can be determined by calculating the angle between the lines light source - target and target - camera. An example for triangulation would be the triangulation based range finder system [1]. Time-of-flight measurements have higher accuracy. In this method, the time that it takes the light to travel from the light source to the target and then to the camera is measured. By multiplying this time with the speed of light, the distance can be calculated. Systems based on this principle are reported in [2, 3, 4]. Interferometric distance measurement offers best length resolution. Coherent laser light is sent to a target and the reflected light interferes with light from a reference.
This thesis shall lay the foundation for developing a 3D sensor with a length resolution of 0.25mm for distances up to 15m in real time. As a first step only one pixel, so regular distance measurement, will be developed. But the focus must be on the development of a system that requires very little hardware so that it can be scaled to a multi-pixel system easily.
There are different interferometric methods [5, 6]. This thesis will focus on the interferometric principle where chirped light from frequency-shifted feedback (FSF) lasers is used. FSF lasers are lasers that have a frequency shifting component in the cavity. Hence, the light gets a frequency shift each round-trip. The development of the FSF lasers and their theory started in the 1990s [7, 8, 9]. Different operation regimes and self mode-locking were discovered [10, 11, 12]. Nakamura *et al.* used a heterodyne beat to perform optical frequency domain ranging [13, 14]. Nakamura *et al.* also proposed the moving comb model [15] to describe the beat signal in dependence of the distance to measure. Detailed calculations of the coherence of FSF lasers were made by Yatsenko *et al.* [16].
The measurement technique with unseeded lasers has the disadvantage of a very low signal-to-noise ratio (SNR). For completeness sake, a possible solution on how to increase the SNR with a seed laser will be mentioned briefly, although this thesis only focuses on unseeded FSF lasers. Yatsenko *et al.* proposed a mathematical description of a seeded FSF laser for distance measurement with higher SNR [17, 18]. The systems with a phase-modulated seed laser show the best SNR and can be implemented using fiber lasers [19, 20, 21]. A nice overview can be found in [16].
In Chapter 2, the theoretical background of the measurement process is discussed. In

the beginning, the focus is to explain why there is a beat signal corresponding to the length to measure and how to generate the chirped light. Then a mathematical and a graphical description of the measurement process are explained. With these models, a possible realization is designed. It shows that a three-dimensional camera with a resolution of 0.25mm and a frame rate suitable for real-time video can be realized with this measurement principle.
Chapter 3 describes how the laser was built. In the beginning of the assembly, there was not sufficient gain and so the gain had to be increased. In the end, there are a couple of pictures of the working laser system.
The measurement results of the laser system are shown in Chapter 4. With the simple electrical measurement principle of resolving each peak in the radio-frequency (RF) spectrum with just one frequency, the resolution was 0.2mm. But when each peak is resolved with more than one frequency, a (much) higher resolution is possible. Since future measurements will require a smaller optical bandwidth, laser line filters were inserted into the cavity to reduce the bandwidth. The implications of measurement with a smaller optical bandwidth are discussed in detail.
In the appendix, there are the detailed calculation of the mathematical model and the calculations for the stability of the laser cavity.

2 Theoretical Background

2.1 Principle of distance measurement with chirped laser light

The goal of this section is to explain how one can measure a distance with chirped laser light. First, there has to be a definition of chirped laser light. In this context, chirped laser light is a coherent light whose frequency increases (or decreases) with time. In general, it is the time dependence of the instantaneous frequency. This does not imply a statement whether this light has a very narrow spectrum or a broad spectrum. The representation of the very narrow spectrum is easier to display, thus the laser light will be displayed as a line in the spectrum (if not stated otherwise). One has to keep in mind that this does not mean that it cannot also have a broad spectrum.

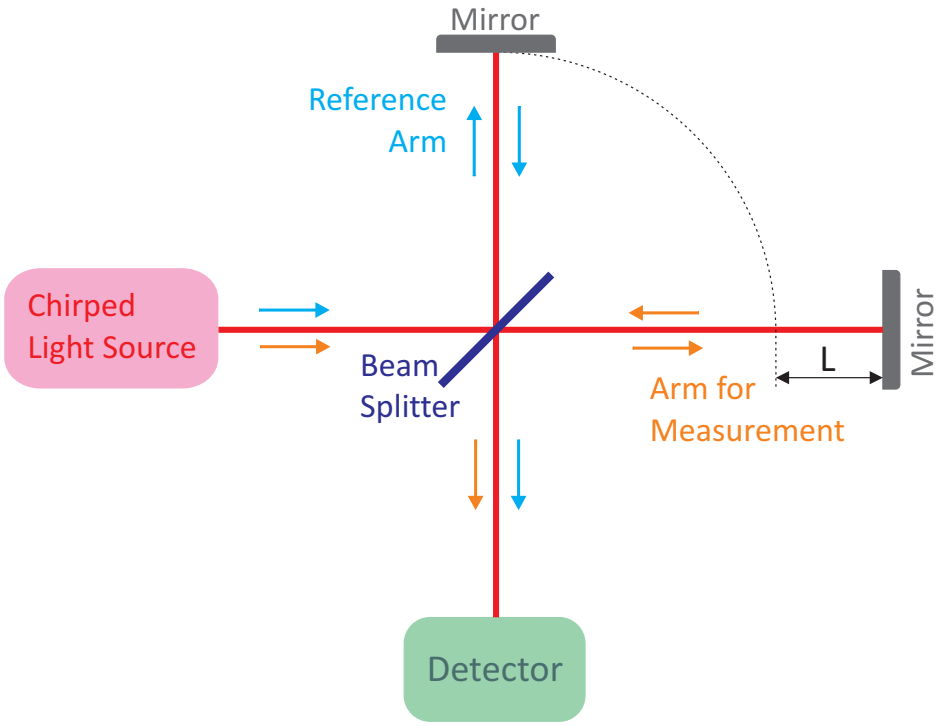

Figure 2.1.: Michelson interferometer

Figure 2.1 shows a Michelson interferometer. There the chirped light is sent to a beam splitter which splits the light into two arms. The first arm, the reference arm, has a known length and will always have a mirror at the end. The second arm, the arm for measurement, contains the length that shall be measured. The length that will be measured is the difference of the lengths of both arms. In this thesis, a mirror will always be at the end of this arm. When building an actual device to measure distances (outside a laboratory), there will be the target instead of the mirror. The light that travels through

the measurement arm is symbolized with orange lines and the light through the reference with blue lines.

One wants to maximize the power from the measurement arm at the detector, assuming that the power from the reference arm will always be high enough, since there will always be a mirror. If the beam splitter has a reflection of R, the power of the measurement arm will be proportional to $(1 - R)R$, because the light has to be transmitted first and then reflected. This term has to be maximized.

$$\begin{aligned} \frac{d\left((1-R)\,R\right)}{dR} &= 1 - 2R = 0 \\ \rightarrow \qquad R &= \frac{1}{2} \end{aligned} \tag{2.1}$$

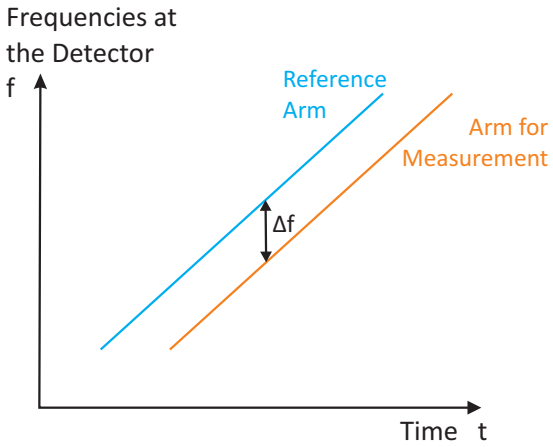

Figure 2.2.: Beat Frequency in a Michelson Interferometer

Hence a 50:50 beam splitter transmits the most power from the measurement arm to the detector. If one assumes the light source creates light with a positive chirp (frequency increases with time), the measured signal at the detector would look something as shown in Figure 2.2. Since the reference arm is shorter, its light will arrive before the light from the other arm does. This time delay will cause a heterodyne beat frequency between the electric fields of the two arms. This frequency is proportional to path difference between the two arms. So by measuring this beat frequency, one will also measure the path difference between the two arms. The length of the reference arm is known. Thus the length of the measurement arm can be calculated easily.

2.2 Generation of chirped laser light

As mentioned in the introduction, this thesis will focus on frequency-shifted feedback (FSF) lasers. A frequency shifted feedback laser is a laser that contains an element in the cavity that shifts the frequency. Therefore, there is no feedback of a frequency to itself after one round-trip and so no longitudinal mode can form inside the cavity. Since the laser has no modes, its spectrum is completely continuous as Nakamura *et al.* [12] demonstrated. The lasing starts at the point in the spectrum where noise is amplified and gets then frequency-shifted with each round-trip.
An acousto-optic modulator (AOM), more exactly an acousto-optic frequency-shifter (AOFS) which is optimized for frequency-shifting, serves as the devices inside the laser cavity that shifts the frequency. What an AOFS does, is that the optical wave, the laser light, gets diffracted at the acoustic wave created in the device. For visible and near-infrared (NIR) light, the AOM-crystal is usually a glass such as SiO_2 or TeO_2. The physical description of this mixing is that the k-vectors of both waves add up and form a new wave. Since the k-vector is proportional to the frequency, this corresponds to an addition or a subtraction of the frequencies. Whether there is a frequency up-shift or down-shift (addition or subtraction) depends on the direction of the optic wave with respect to the acoustic wave. Principally, the light wave is always nearly perpendicular to the acoustic wave. If a part of the optic wave has the same direction as the acoustic wave, the resulting light wave will have a lower frequency (frequency down-shift). If a part of the optic wave has the opposite direction as the acoustic wave, the resulting light wave will have a higher frequency (frequency up-shift). That can be seen in Figure 2.3.

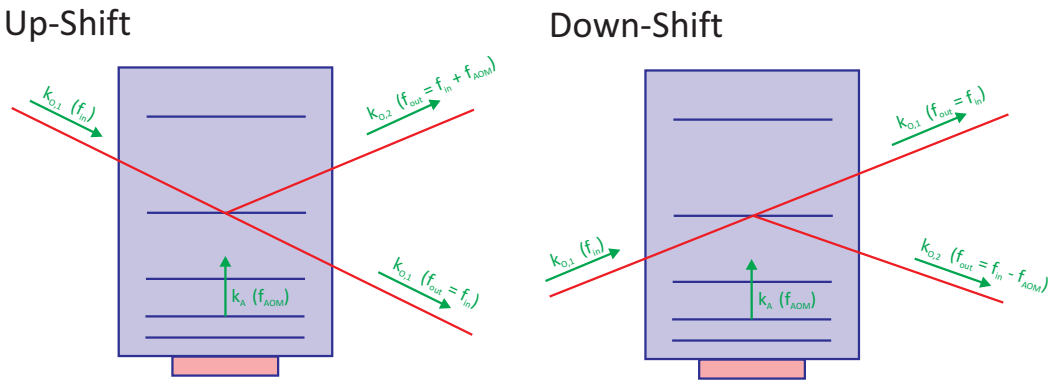

Figure 2.3.: Frequency up-shift and down-shift due to an AOFS

There are two types of AOFS, one that has a standing acoustic wave in it and one that has a traveling acoustic wave in it. A standing wave can be interpreted as two waves traveling in opposite direction. Hence with a standing wave AOFS, parts of the resulting wave will be up-shifted and other parts of the resulting wave will be down-shifted. Since the FSF laser requires either a frequency up-shift or down-shift but not both, one has to

choose a traveling wave AOFS.

In a normal laser, there is always the boundary condition that the round-trip length of the laser cavity is always an integer multiple of the wavelengths in the cavity. This condition does not apply to FSF lasers because the light in the cavity will be frequency-shifted each round-trip. So the light of one specific frequency will not give feedback to itself. It will only influence the neighboring shifted frequency. This leads to the behavior that modes cannot form in the cavity and the spectrum is completely continuous, as already mentioned. The other condition of normal lasers that the gain has to exceed the losses, of course, applies to FSF lasers as well.
One possibility to build an FSF laser is using a linear cavity. The principle setup can be seen in Figure 2.4.

The lasing medium provides the gain and the AOFS provides the frequency shift. In

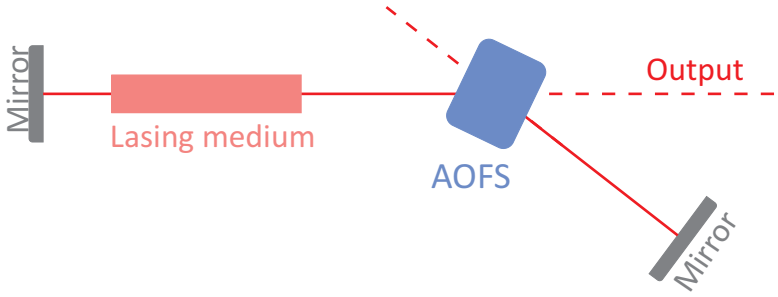

Figure 2.4.: FSF laser in a linear cavity setup

this setup, the light passes through the AOFS twice each round-trip. Thus the frequency shift per round-trip is two times the AOM frequency. The undiffracted beam (0^{th} order diffraction) will exit the cavity and will therefore contribute to the losses. Hence, there are two beams that can be used as output beams. The light will also pass twice through the lasing medium and thereby the lasing medium has to provide enough gain to compensate for all the losses.
Another possibility to build an FSF laser is with a ring cavity. This scheme is shown in Figure 2.5. Here the light passes only once per round-trip through the AOFS and the

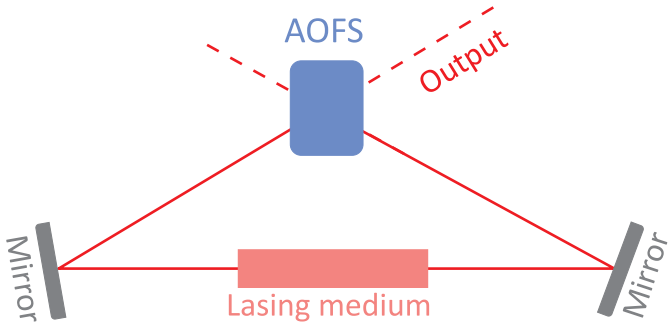

Figure 2.5.: FSF laser in a ring cavity setup

lasing medium. Therefore the frequency shift per round-trip corresponds to the AOM

frequency. In this setup, the light can travel in both directions. Thus there are again two possible output beams. If one inserts a Faraday isolator into the cavity, the light will only be able to travel in one direction and there will only be one output beam. The disadvantage of the setup with a Faraday isolator is that the threshold power will not drop but (slightly) increase because of the (small) losses introduced into the cavity. To further explain this behavior, if there is no lasing, fluorescence will be sent in all directions and only if enough light is reflected back to the crystal, the lasing will start. But after lasing has started, the output power will increase faster with more pump power than without the isolator, because the main energy is only consumed by light in one direction.

2.3 Mathematical description of the system

2.3.1 On mathematical description of the system

In [16], Yatsenko *et al.* show that in the spectrum, there is something like a source that produces one single frequency with a constantly varying phase, except for stochastic changes in this phase. This frequency is shifted after each round-trip and thus behaves similar to a comb. To get a continuous spectrum, one can image that there are peaks of other combs in between two comb peaks. The combination of all these combs then forms the continuous spectrum of the FSF laser.

As an approximation for this system, one can use the moving comb model introduced by

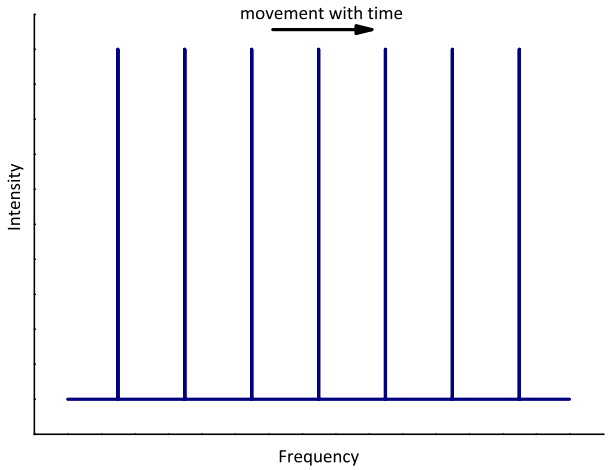

Figure 2.6.: Scheme of moving comb model

Nakamura *et al.* [15]. This model assumes that a comb of frequencies separated by the frequency shift per round-trip experiences a continuous frequency shift in time. Therefore the spectrum of the comb will move with time, see Figure 2.6. This is only an approximation because the chirp in an FSF laser is not continuous but discrete, and the spectrum of an unseeded FSF laser is continuous but does not consist of a discrete comb. It is mathematically easy to describe and delivers good theoretical results corresponding nicely to

measured results.

2.3.2 Definitions

The chirp rate is constant. The frequency increases by the AOM frequency f_{AOM} each round-trip (round-trip time T_R) in a ring cavity. In a linear cavity, it increases by $2f_{AOM}$ each round-trip. The chirp rate σ can be defined as $\sigma = \frac{f_{AOM}}{T_R}$ for a linear cavity or $\sigma = 2\,\frac{f_{AOM}}{T_R}$ for a ring cavity. In the following, only a ring cavity will be calculated. Hence,

$$\sigma = \frac{f_{AOM}}{T_R} \quad . \tag{2.2}$$

For the calculations of the linear cavity refer to the appendix A.1.2. With the chirp, one can write the phase φ_q of mode-index q as

$$\varphi_q(t) = \frac{c_0}{\lambda}\left(t - \frac{q}{f_{AOM}}\right) + \frac{\sigma}{2}\left(t - \frac{q}{f_{AOM}}\right)^2 + \phi_q \tag{2.3}$$

where $\frac{c_0}{\lambda}$ corresponds to starting frequency and ϕ_q a constant phase offset for each round-trip. Accordingly, λ is the starting wavelength. And the $\left(t - \frac{q}{f_{AOM}}\right)$ terms guarantee that the comb peaks are separated by f_{AOM}. Hence, the frequency f_q of each mode can be calculated easily as

$$f_q(t) = \frac{d\varphi_q(t)}{dt} = \frac{c_0}{\lambda} + \sigma\left(t - \frac{q}{f_{AOM}}\right) \quad . \tag{2.4}$$

Figure 2.7 shows the linear frequency chirp of the modes over time, where n and p are integer numbers.

The electric field consists of N modes and can be written as

$$E(t) = \sum_{q=1}^{N} E_q(t)\; e^{i\,2\pi\varphi_q(t)} \tag{2.5}$$

where $E_q(t)$ is the amplitude of the mode and is always real. Usually people define a Gaussian spectral envelope which has to be modeled into this term. The Gaussian envelope makes things like a Fourier transform easier and it corresponds nicely with the measured spectrum. In the following, the shape of the amplitude envelope does not matter, so the term $E_q(t)$ will not be further defined. It will just be treated as any (arbitrary) amplitude.

The intensity of the FSF laser can be calculated as

$$I(t) = \frac{nc_0\epsilon_0}{2}\,|E(t)|^2 \quad . \tag{2.6}$$

One of the arms of the Michelson interferometer is longer by L than the other arm. This fact will result in a time delay of $\frac{2L}{c_0}$ in one of the electric fields. The intensity after the

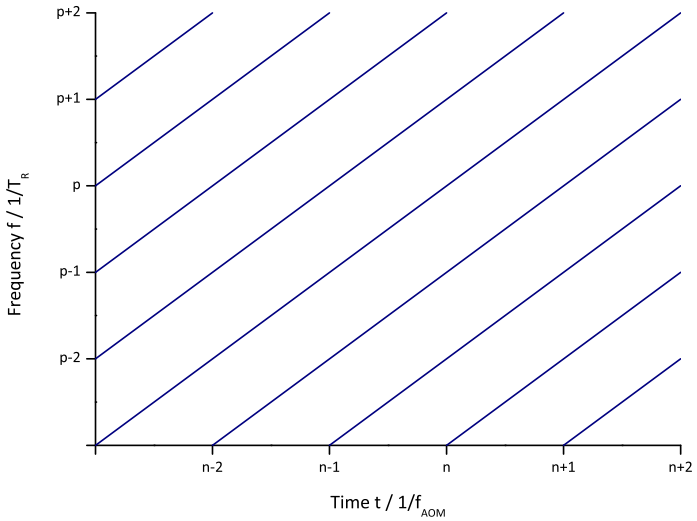

Figure 2.7.: Evolution of frequencies over time in the moving comb model

Michelson interferometer is then

$$\begin{aligned} I\left(t\right) &\propto \left|\delta\, E\left(t\right) + \eta\, E\left(t - \frac{2L}{c_0}\right)\right|^2 \\ &= \delta^2 \left|E\left(t\right)\right|^2 + \delta\eta \left|E^*\left(t\right)\; E\left(t - \frac{2L}{c_0}\right) + E\left(t\right)\; E^*\left(t - \frac{2L}{c_0}\right)\right| + \eta^2 \left|E\left(t - \frac{2L}{c_0}\right)\right|^2 \end{aligned} \tag{2.7}$$

where δ and η are the losses in the two arms.

2.3.3 Analytic results

For a detailed calculation, refer to the appendix A.1.1. At first, the three terms from Eq. (2.7) are calculated separately. The intensity can then be written as

$$I(t) \propto I_1(t) + I_2(t) + I_3(t) \quad . \tag{2.8}$$

When calculating the first term, one has to remember that the multiplication of a sum (2.5) with a sum can be written as a sum of sums. Therefore one can define a beat index p. This beat index just denotes what harmonic of the beat frequencies one refers to. The result of the first term can be seen in the following equations:

$$I_1(t) = \delta^2 \left|E\left(t\right)\right|^2 = \delta^2 \sum_{p=0}^{N-1} \sum_{q=1}^{N-p} E_q\left(t\right)\; E_{q+p}\left(t\right)\; \cos\left(2\pi\left(f_{beat,1}(q,p)\, t + \varphi_{beat,1}(q,p)\right)\right) \tag{2.9}$$

$$f_{beat,1}(q,p) = \frac{p}{T_R} \tag{2.10}$$

$$\varphi_{beat,1}(q,p) = \frac{c_0}{\lambda}\, \frac{p}{f_{AOM}} - \frac{\sigma}{2}\, \frac{2qp + p^2}{\left(f_{AOM}\right)^2} + \phi_q - \phi_{q+p} \tag{2.11}$$

The first term is the autocorrelation of the light from the reference arm and so the result is not surprising. In Figure 2.7, one can see that the modes are separated by $\frac{1}{T_R}$. Thus the resulting beat frequencies are an integer multiple of $\frac{1}{T_R}$. The phases have to be an integer multiple of 2π in order to get constructive interference of all the modes. But that is, of course, valid for all terms.
For the second term, one can use the same scheme to calculate the beat frequencies.

$$\begin{aligned} I_2(t) &= \delta\epsilon \left| E^*(t)\ E\left(t-\frac{2L}{c_0}\right) + E(t)\ E^*\left(t-\frac{2L}{c_0}\right)\right| = \\ &= \delta\epsilon \left(\sum_{p=0}^{N-1} \sum_{q=1}^{N-p} E_q(t)\ E_{q+p}\left(t-\frac{2L}{c_0}\right) \cos\left(2\pi\left(f_{beat,2a}(q,p)\,t + \varphi_{beat,2a}(q,p)\right)\right) \right. \\ &\quad \left. + \sum_{p=0}^{N-1} \sum_{q=1}^{N-p} E_{q+p}(t)\ E_q\left(t-\frac{2L}{c_0}\right) \cos\left(2\pi\left(f_{beat,2b}(q,p)\,t + \varphi_{beat,2b}(q,p)\right)\right) \right) \end{aligned} \tag{2.12}$$

$$f_{beat,2a}(q,p) = \frac{1}{T_R}\left(p + \frac{2\,f_{AOM}}{c_0}\ L\right) \tag{2.13}$$

$$\varphi_{beat,2a}(q,p) = \frac{2L}{\lambda} + \frac{c_0}{\lambda}\,\frac{p}{f_{AOM}} - \frac{\sigma}{2}\left(\left(\frac{2L}{c_0}\right)^2 + \frac{4L}{c_0}\,\frac{q+p}{f_{AOM}} + \frac{2qp+p^2}{(f_{AOM})^2}\right) + \phi_q - \phi_{q+p} \tag{2.14}$$

$$f_{beat,2b}(q,p) = \frac{1}{T_R}\left(p - \frac{2\,f_{AOM}}{c_0}\ L\right) \tag{2.15}$$

$$\varphi_{beat,2b}(q,p) = \frac{\sigma}{2}\left(\left(\frac{2L}{c_0}\right)^2 + \frac{4L}{c_0}\,\frac{q+p}{f_{AOM}} - \frac{2qp+p^2}{(f_{AOM})^2}\right) - \frac{2L}{\lambda} + \frac{c_0}{\lambda}\,\frac{p}{f_{AOM}} + \phi_q - \phi_{q+p} \tag{2.16}$$

The results for the beat frequencies show a dependence on the length difference L of the two arms because the second term is a correlation of the light from both arms. There is one term that shows length dependence proportional to L, Eq. (2.13), and another term with a length dependence proportional to $-L$, Eq. (2.15). Those are the terms that are most interesting because they contain information on the length L that one wants to measure.
There is an ambiguity because of the constant offset from the beat index. The unambiguous range L' is defined as

$$L' = \frac{c_0}{2\,f_{AOM}} \quad . \tag{2.17}$$

That means it is not possible distinguish between $L_1 = L_0$ and $L_2 = L_0 + n\,L'$, where n is an integer. The reason is that L_2 would correspond to L_1 with a different beat index ($p_2 = p_1 + n$). There is one other thing that one has to keep in mind. The beat index p is always an integer from $-(N-1)$ to $N-1$. In the first term $I_1(t)$ (and the third term $I_3(t)$), there is a symmetry and the sums $\sum_{p=0}^{N-1}$ and $\sum_{p=-(N-1)}^{0}$ were transformed to $2\sum_{p=0}^{N-1}$. In the second term $I_2(t)$, the length L causes an offset for p if $L < 0$ or $L >= L'$. Hence, the exact range of p depends on L. In this thesis, we will restrict ourselves to $0 \leq L < L'$

without limiting the generality. If one wants to calculate different lengths, one only has to adapt the beat index p accordingly.
Because of the term $\frac{p}{T_R}$ with the mode index p, there is an ambiguity in frequency, too. This measurement principle with ambiguity in frequency and length is also called optical frequency domain ranging. A big advantage of this principle is the constant length resolution. That means the resolution is constant no matter if one measures 1m or 10km. The third term is similar to the first one, and the results are:

$$I_3(t) = \epsilon^2 \left| E\left(t - \frac{2L}{c_0}\right)\right|^2 = \epsilon^2 \sum_{p=0}^{N-1} \sum_{q=1}^{N-p} E_q\left(t - \frac{2L}{c_0}\right) E_{q+p}\left(t - \frac{2L}{c_0}\right) \cdot \cdot \cos\left(2\pi \left(f_{beat,3}(q,p)\, t + \varphi_{beat,3}(q,p)\right)\right) \tag{2.18}$$

$$f_{beat,3}(q,p) = \frac{p}{T_R} \tag{2.19}$$

$$\varphi_{beat,3}(q,p) = \frac{c_0}{\lambda}\frac{p}{f_{AOM}} - \frac{\sigma}{2}\left(\frac{p}{f_{AOM}}\frac{4L}{c_0} + \frac{2qp+p^2}{(f_{AOM})^2}\right) + \phi_q - \phi_{q+p} \tag{2.20}$$

The third term is again an autocorrelation. In this case, it is the autocorrelation of the light from the measurement arm. The result is basically the same as the first term, except for a slightly different phase term due to the different length.

2.3.4 Graphical solution

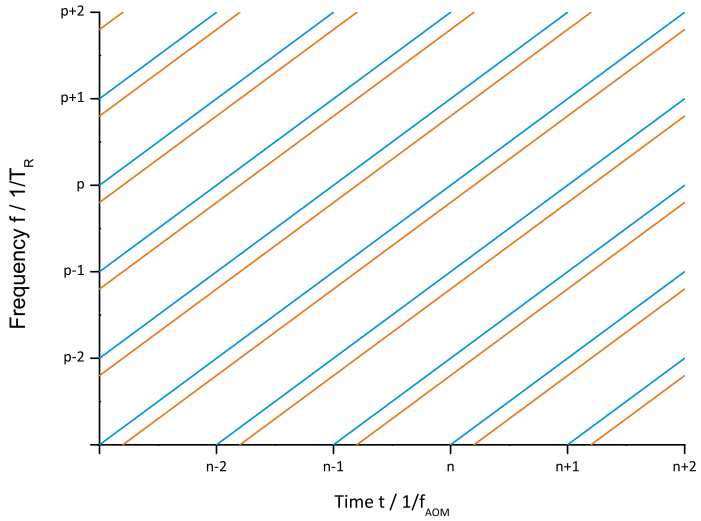

Figure 2.8.: Resulting frequencies after the Michelson interferometer

Of course, it is necessary to have an exact mathematical solution for the beat frequencies. However, there is an easy-to-understand graphical solution. As can be seen in Figure 2.7, the modes are separated by $\frac{1}{T_R}$ in the frequency domain and by $\frac{1}{f_{AOM}}$ in the time domain. If this light is sent into a Michelson interferometer and the two arms have different length, the result will be that the same frequencies appear a second time but only shifted in time,

corresponding to the time difference, as can be seen in Figure 2.8.
The same colors as in Figure 2.1 were used, where blue matches with the reference arm and orange with the measurement arm. In this figure, n and p are arbitrary integer numbers. The same issue is handled in Figure 2.9 which is a zoom of the last figure. The beat frequencies are labeled this time, though.

$f_{beat,1}(p = 0)$ and $f_{beat,3}(p = 0)$ are the autocorrelations and are represented with the

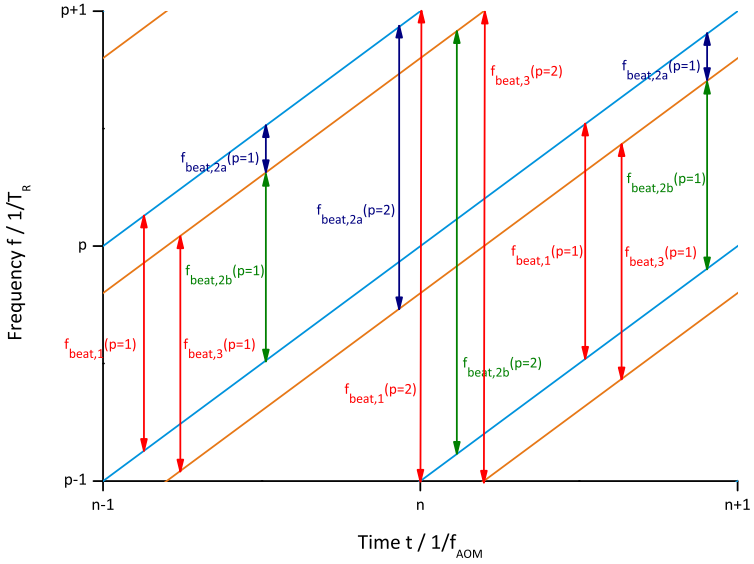

Figure 2.9.: Zoom of resulting frequencies after the Michelson interferometer with beat frequencies

color red. As the distance L increases the position of the orange lines will move to the right. Therefore, $f_{beat,2a}(p = 0)$ is from a blue line to the next orange line below and it shows the length dependence of this beat frequency. One can also see the ambiguity quite clearly. If the orange lines move further to the right, they will collide with the neighboring blue lines. So it cannot be determined to what blue line an orange line belongs.
$f_{beat,1}(p = 1)$ and $f_{beat,3}(p = 1)$ are the correlation of the neighboring lines with the same color. $f_{beat,2b}(p = 1)$ is the opposite of $f_{beat,2a}(p = 0)$ because it has a negative length dependence. Together they sum up to $f_{beat,2a}(p = 0) + f_{beat,2b}(p = 1) = f_{beat,1}(p = 0) = f_{beat,3}(p = 0)$. In the figure, the second harmonics can be seen too. In theory, one can apply this pattern and easily show higher harmonics, too.

Figure 2.10 shows the resulting beat frequencies in dependence of the distance L. The frequencies are scaled with $\frac{1}{T_R}$, and the length is scaled by the factor L'. One can easily see the ambiguities in length and in frequency. The same frequencies repeat every L' in length, but they also repeat every $\frac{1}{T_R}$ in the frequency domain (hence, optical frequency domain ranging).

Since the green and the blue lines are not independent of each other, the ambiguity is even stronger. If we take just the region from 0 to $\frac{1}{T_R}$ in the frequency domain and from 0 to L' in length, as can be seen in Figure 2.11. Let us consider, we measure the frequency F_0 which on the green line corresponds to the length L_0. But we can only

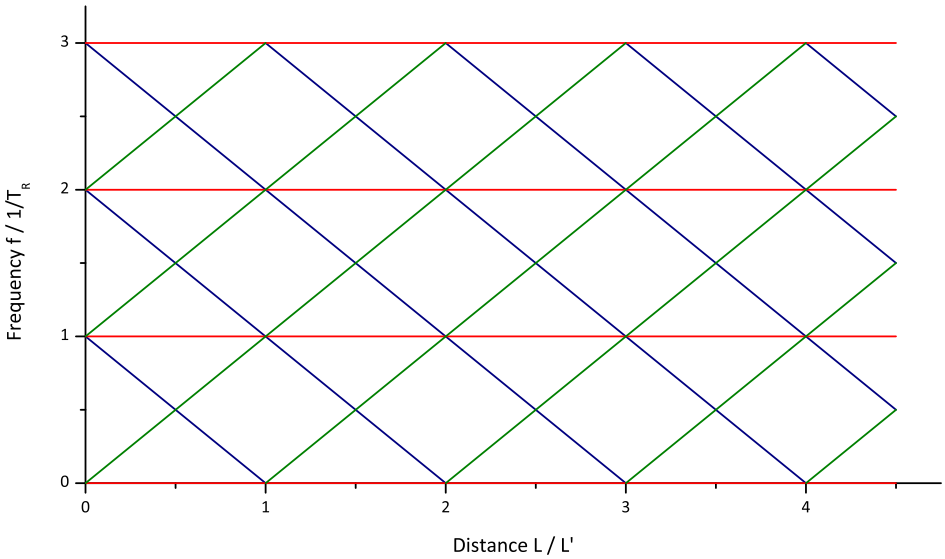

Figure 2.10.: Resulting beat frequencies versus distance L

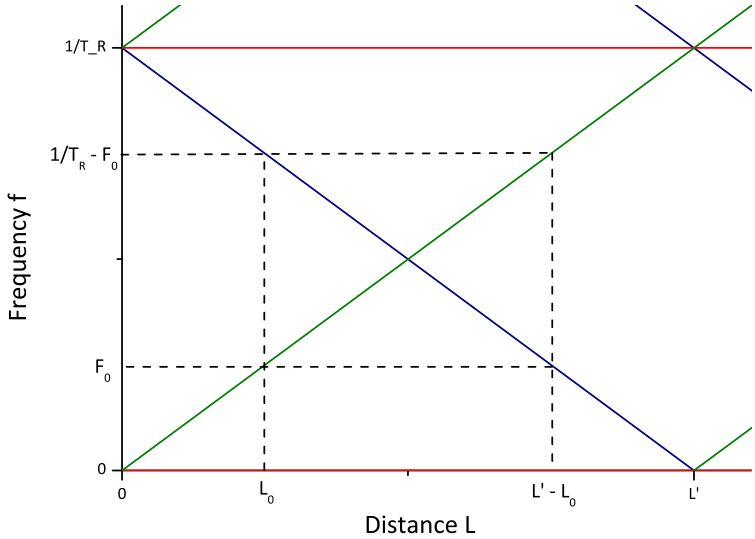

Figure 2.11.: Zoom of resulting beat frequencies versus distance L

measure frequencies, so we do not know if the frequency corresponds to the green or the blue line. Therefore we might also measure the distance $L' - L_0$. And if we measure F_0, we will always measure the frequency $\frac{1}{T_R} - F_0$ too. So we can split our region 0 to $\frac{1}{T_R}$ and 0 to L' in four quadrants, each has half the frequency range and half the length of the original region. So the actual unambiguous range is $\frac{1}{2T_R}$ in the frequency domain and $\frac{L'}{2}$ in length.

We have to get rid of the ambiguity too in order to measure absolute distances. We could try to measure different frequencies for the same lengths by changing the cavity. But that would require a very complicated laser. Hence, it is not a good option. Another option would be to change the AOM-frequency. That results in different L's for different frequencies which can be seen in Figure 2.12. Then the ambiguity can be resolved by comparing all possible lengths due to ambiguity of the first AOM-frequency with all possible lengths due to ambiguity of the second AOM-frequency. Only in one length

they will match and that is the correct length. That assumes, of course, that the two AOM-frequencies are chosen wisely (close to each other). For example, doubling the AOM-frequency will help only very little to resolve the ambiguity.

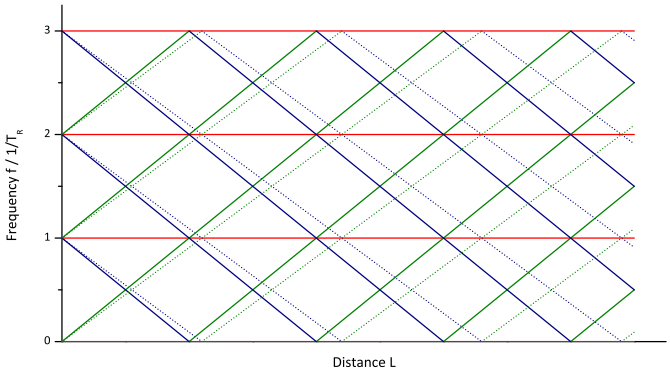

Figure 2.12.: Getting rid of the ambiguity by changing the AOM frequency

2.4 Designing the laser system

Before we can start designing the actual laser system[1], we have to think about what we want to build. The aim is building a laser system that allows to build a 3D-camera with a resolution of 0.25mm and real-time video frame rate. The distance range is 0 to 15m. The hardware requirements for each pixel shall be as small as possible. The circuits with the smallest hardware requirements are comparators. These compare the measured frequency to a reference frequency and decide if they are the same. The highest frequencies shall not be too high, and the wavelength shall be detectable with standard silicon photodiodes.

The first decision to make is the type of laser. A titanium:sapphire (Ti:Sa) laser was chosen because Ti:Sa lasers have a huge bandwidth and are detectable with silicon photodiodes.
The highest frequency to measure was set to 100MHz. And since the unambiguous range in frequency is $\frac{1}{2T_R}$, one could build a laser with $\frac{1}{T_R} = 200\text{MHz}$. This laser would require to measure very low frequencies and frequencies over more than eight orders of magnitude, though. That is not desired. Hence, we build a laser with $\frac{1}{T_R} = 100\text{MHz}$ ($T_R = 10\text{ns}$). Then we could measure either frequencies from 0 to 50MHz, or from 50 to 100MHz. The latter allows doing the required frequency measurement within just one octave and the frequencies are not so low that their measurement would take long.

[1] In this chapter, we will only estimate a feasible system. Therefore small error regarding powers of 2 are neglected, e.g., $1000 \approx 1024$.

The next decision is the AOFS. AOFS are available from about 10MHz to a couple of 100MHz. The higher the AOFS frequency is, the shorter the unambiguous range in length is. A shorter unambiguous range requires fewer comparisons with reference frequencies for the same length resolution and that corresponds to a higher frame rate. A disadvantage of a shorter unambiguous range and fewer frequency steps is that the ambiguity can only be resolved for shorter lengths. The longest distance is 15m and therefore rather short, so that should not cause any problems. Hence, a high AOFS frequency of 300MHz was chosen. That corresponds to $L' = 0.5$m and the unambiguous range $\frac{L'}{2} = 0.25$m.
The measured frequency can be assumed to be monochromatic. In order to decide whether the frequency was measured correctly or not, the frequency has to be compared with a frequency band. Since the resolution shall be 0.25mm, we have to divide the unambiguous range in 1024 frequency bands.

When comparing the frequency with the frequency bands, using non-overlapping fre-

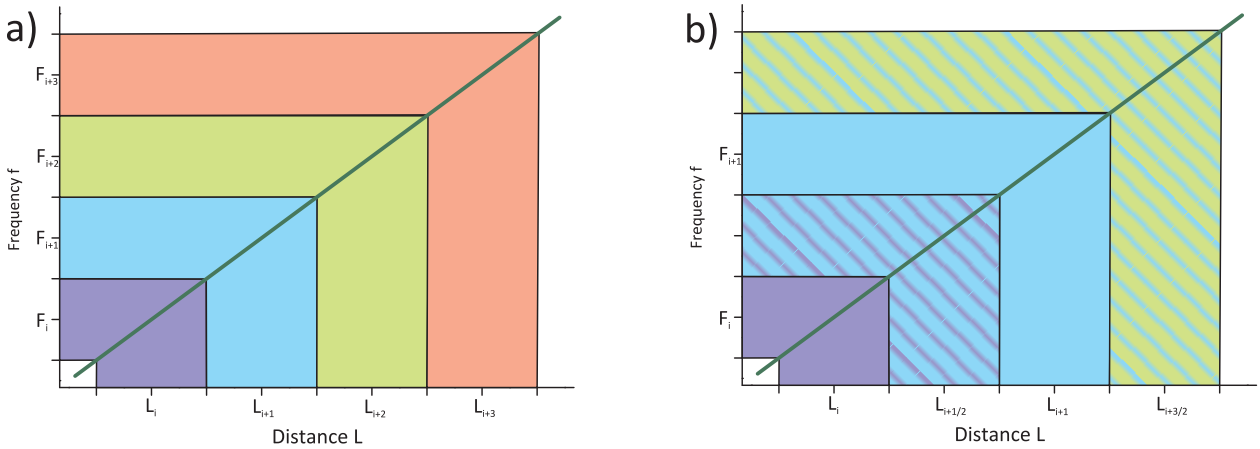

Figure 2.13.: Measuring only half as many frequencies through overlap

quency bands (Figure 2.13 a) has disadvantages. If the frequency is just at the border of two frequency bands, the frequency might not be detected or might be detected for both neighboring frequency bands. To solve this problem, one can use overlapping frequencies (Figure 2.13 b). In this scheme, the frequency bands overlap. Their width is thrice as big and the distance to the neighbor is twice as big. All frequency bands together cover the whole range and the frequency to measure will definitely be detected. Therefore, only small errors are possible, when the frequency is at the edge of one of the frequency bands. Since the distance to the neighbor is twice as big, only half as many frequency bands and thus comparisons are necessary. Hence, one measurement cycle will be faster.
The distance range L_i corresponds to the purple frequency band (only F_i is detected). The neighbor $L_{i+1/2}$ is associated with the overlap of the purple and the blue regions (F_i and F_{i+1} are detected). These two patterns alternate for all distance ranges, as can be seen also for L_{i+1} (blue region) and $L_{i+3/2}$ (blue and green region). A disadvantage of this scheme is that it requires slightly more hardware.
When applying this scheme we will need 512 frequency bands, and thus comparisons. The whole frequency range was from 50 to 100MHz. Therefore, one frequency band will have

a width of $\frac{50MHz}{512} \approx 100$kHz.
The next thing we need to estimate is the required optical bandwidth. In general, the more optical bandwidth there is, the smaller the bandwidth of the beat signal will be. That fact can be seen as that more lines interfere with each other and the beat will be defined more precisely. So, we want as much bandwidth as possible.
There is one downside, though. In the laser system discussed in this thesis, noise is mixed with noise and the resulting beat signal contains the length information. Obviously, the signal to noise ratio (SNR) will be very low. There are ways to increase the SNR with a seed laser and phase-modulation, as proposed by Yatsenko *et al.* [18]. But for this scheme, the light for each measurement has to be created. Therefore after the generation one has to wait for the light to cover the whole bandwidth. So, the more bandwidth one uses, the longer one will have to wait and that will result in a slower measurement process. In this thesis, we will still just treat the unseeded laser system. But since the final system will contain a seed laser with phase-modulation, too, we have to take that in consideration when estimating the resulting frame rate.

$$\Delta f_{beat} = \frac{2}{T_R N'} \tag{2.21}$$

Eq. (2.21) corresponds to Eq. (37) of [18]. $T_R N'$ corresponds to the Gaussian width, assuming Gaussian spectral amplitude distribution. We can approximate them as cavity round-trip time times number of round-trips in the cavity. Our beat signal must be smaller than 100kHz with a repetition (cavity) frequency of 100MHz. Therefore, we will need about 2000 round-trips in the cavity.[2]
If we assume an AOM frequency of 300MHz and 2000 round-trips, that results in an optical bandwidth of 600GHz. At a wavelength of 780nm, a bandwidth of 600GHz corresponds to about 1.2nm. But 1000 round-trips will probably already be enough. That would result in a bandwidth of 300GHz or 0.6nm (at 780nm).
In order to calculate how long a measurement cycle will last, we need to know how long the electrical measurement will take. We have to distinguish between frequencies with a resolution of 100kHz. Let us imagine, we want to discriminate 68.2MHz from 68.3MHz. One could count the number of cycles of the frequency to measure. During a time of $\frac{1}{100kHz}$ $= 10\mu$s, one would count either 682 or 683. Hence one can distinguish the frequencies. But if one miscounts because of noise on the signal, another (wrong) signal will be detected. Therefore, it is smart to count for a longer duration. For example, if the time is set to 20μs, one has to miscount at least twice to detect another signal. Note: The durations mentioned here are all just theoretical and can only be seen as estimates. When building the actual circuits, one has to measure the exact durations depending on the noise level.
If we build the laser for 1000 round-trips of light in the cavity, we have to wait for 10μs before we can start the electrical measurement. After another 10μs, the measurement cycle for one frequency is completed. Thus, checking one distance (for one AOM frequency)

[2] If we use a narrow bandwidth seed, the bandwidth of the beat will decrease. Then, the beat signal can be treated as being monochromatic, as previously assumed.

takes 20μs. We have to check 512 frequencies in the unambiguous range. After that we can change the AOM frequency and recheck the 512 frequencies in order to resolve the ambiguity. Over all, we have to check 1024 frequencies which will take about 20ms. That results in a frame rate of the camera of about 50 frames per second. If we build the laser system more conservatively for 2000 round-trips of light in the cavity and electrical measurement duration of 20μs, measuring the 1024 frequencies will take 40ms which will result in a frame rate of 25 frames per second.

3 FSF Laser

3.1 Equipment

Most of the equipment needed was available at the Institute of Photonics. As pump laser, we used a **Verdi-V5** from *Coherent*. We had two different Ti:Sa crystals. The first was 2.0mm long and the second 2.9mm. High reflecting mirrors for 800nm were available.
The only thing that had to be ordered was the AOFS. The **MT300-B20A0.5-800** from the company *AA Opto-Electronic* with parameters listed below was chosen.

- 700-950nm, linear polarization
- optical transmission: >98%
- carrier frequency 300MHz ± 10MHz
- aperture 0.5x2mm^2
- recommended beam diameter 0.3mm
- rise time 160ns/mm
- maximum RF power 1.5W
- diffraction efficiency
  - >80% (typically 85%) at 300MHz
  - >70% (typically 75%) in the range from 290 to 310MHz

3.2 Measuring the AOFS efficiency

The efficiency of the AOFS has a big impact on the FSF laser. The higher the efficiency is, the less gain is needed to get lasing. That implies of course, for an AOFS with poor efficiency one will need very high gain to get lasing. Therefore we measured the efficiency of the AOFS to get an idea of how much gain we will need.
The efficiency of an AOFS is defined as

$$\text{Efficiency in \%} = 100\,\frac{\text{Optical power in } 1^{st} \text{ order diffraction with RF-power}}{\text{Optical power in } 0^{th} \text{ order diffraction without RF-power}}\ .$$

In order to measure the efficiency, a laser had to be built. The setup can be seen in Figure 3.1. Already using the Ti:Sa crystal in this setup has the advantage that the wavelength

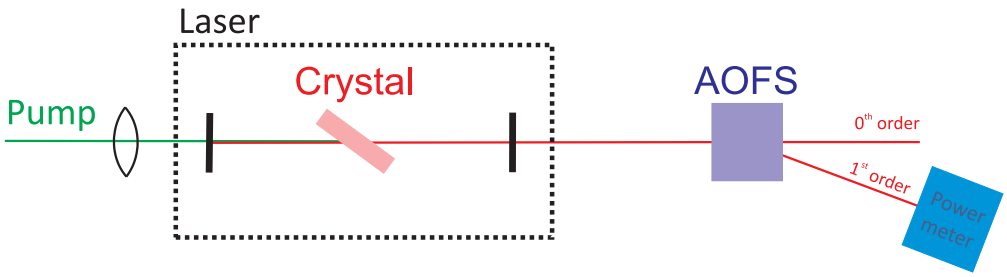

Figure 3.1.: Setup to measure the AOFS efficiency

is (approximately) the same as the wavelength that will be produced by the FSF laser. At first, the transmission ("Optical power in 0^{th} order diffraction without RF-power") was measured. Then the AOFS was turned on and the optical power in the 1^{st} order diffraction was measured.

The highest measured efficiency was at an RF power of 1.5W and was 67%, as can be

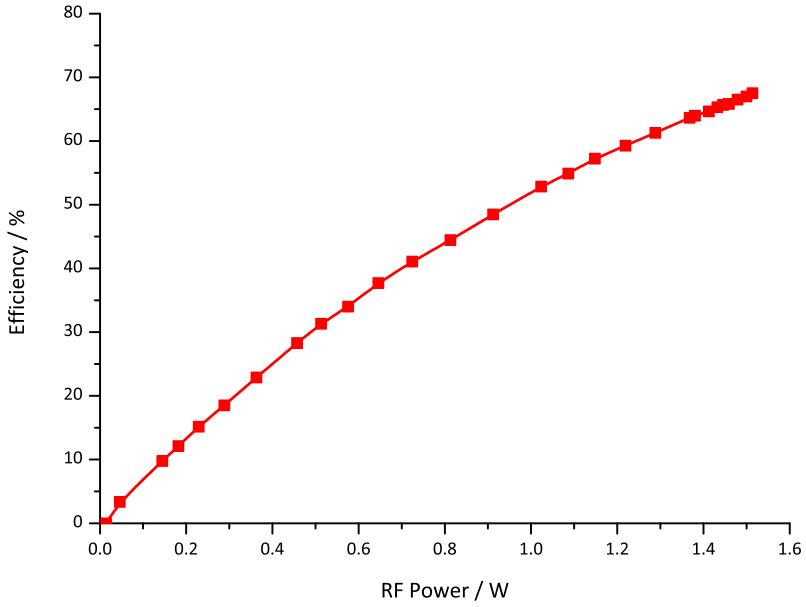

Figure 3.2.: Measured AOFS efficiency in dependence of the RF power

seen in Figure 3.2. That means that we will lose about one third of all photons each round-trip at the AOFS. Unfortunately, we could not reach the 80% that were promised by *AA Opto-Electronic*. One can easily extrapolate from the graph that if we were to turn up the RF power to more than 1.5W, we would observe higher efficiencies. But higher powers could damage the transducer in the AOFS and thus we are limited to 67%.

Note: In future systems, one should think about the required frequency. The lower the attenuation of the acoustic wave in the AOFS is, the higher the AOFS efficiency will be. The attenuation of an acoustic wave in a solid is proportional to the square of the frequency, as described in Eq. (3.83) of [23]. So the higher the frequency is, the higher the attenuation is and therefore the lower the efficiency is. There are AOFSs with efficiencies

higher than 90% available at about 100MHz. Hence, less gain will be needed with such an AOFS, and the laser threshold will drop.

3.3 Too little gain

When building a laser and if one does not know if there is enough gain to reach the lasing threshold, there is the problem that if the laser is not lasing, it will be tough to find the problem. One could align everything perfectly but if the gain does not suffice, there will be no lasing. Or one could have misaligned something, so there is no lasing. To solve this problem, one can build an auxiliary cavity that has to be similar to the FSF laser cavity. This means that the stability zones have to overlap and one could use iris apertures to match the beam of the FSF laser with the one of the auxiliary cavity. The principle alignment of the auxiliary cavity built for the FSF laser can be seen in Figure 3.3. The Ti:Sa crystal is aligned under Brewster angle and thus the laser will produce light

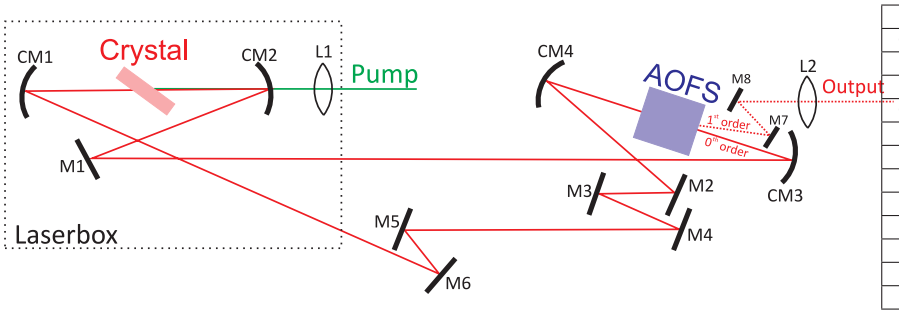

	Length / mm
CM1 - CM2	50
CM2 - M1	42
M1 - CM3	1315
CM3 - CM4	430
CM4 - M2	420
M2 - M3	235
M3 - M4	120
M4 - M5	800
M5 - M6	40
M6 - CM1	415
Sum	3867

Figure 3.3.: Auxiliary cavity to align the beam path

with horizontal polarization. The two curved mirrors around the crystal (CM1, CM2) have both a focal length of 25mm and are transparent for the pump light at 532nm. The aperture in the AOFS is rather small and in order to reach high AOFS efficiencies, a small beam diameter is required. Therefore the beam has to be focused into the AOFS. The focal length of the curved mirrors CM3 and CM4 is 200mm. The 2.9mm Ti:Sa crystal was chosen. The crystal of the AOFS is made of tellurium dioxide and is 30mm thick.
In the next step, one must check if the laser is actually stable. Therefore, we can have a look at the stability zones of Figure 3.4.

Both the crystal and the AOFS have to be close to the focal point of the curved mirrors. Hence, the distance Crystal-CM2 was chosen as 24.3mm and the distance AOFS-CM4 as 200mm. The other two lengths in the focal regions (CM1-Crystal, CM3-AOFS) were varied. The stability for every variation of the two lengths was calculated with the ABCD-matrix formalism described in Chapter A.2.
One can see the two stability zones. Since we want to focus the beam into the Ti:Sa and the AOFS crystal, we need to choose lengths that are close to the focal lengths of the curved mirrors. The dependence on the length CM3-AOFS is weaker than that of CM1-Crystal because the focal length of CM3 is longer than that of CM1. Therefore, we set the

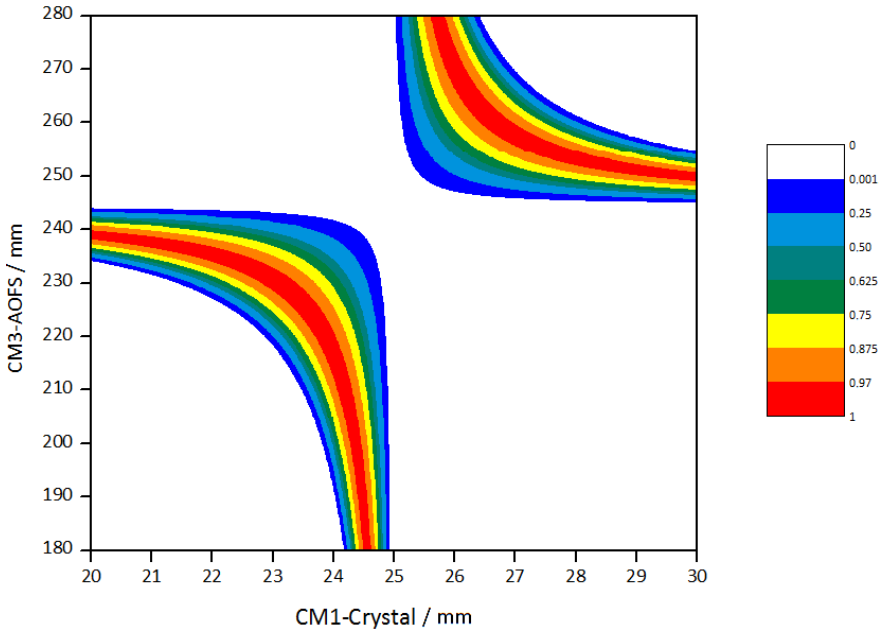

Figure 3.4.: Stability zones of the laser

distance CM3-AOFS to 200mm and look at the stability in dependence of CM1-Crystal, as can be seen in Figure 3.5.

Theoretically, the laser will be stable if the calculated stability is greater than zero. In

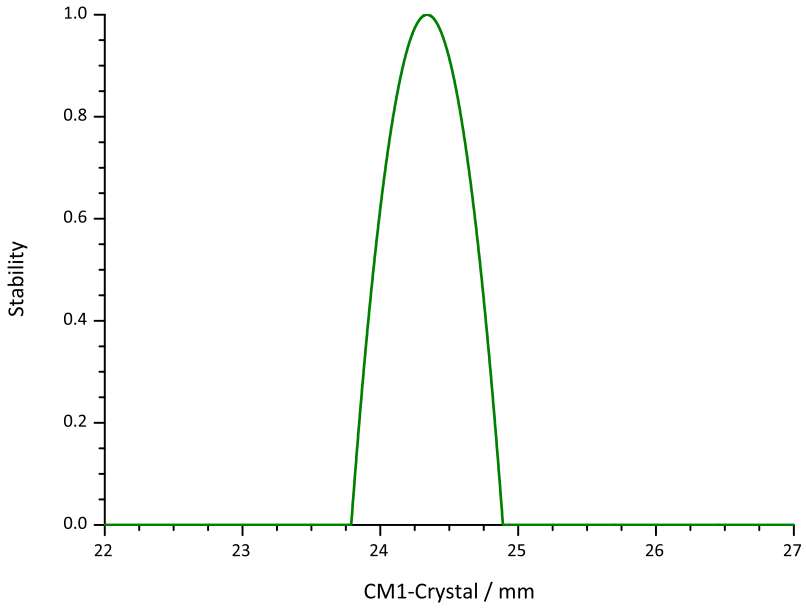

Figure 3.5.: Stability of the laser in dependence of CM1-Crystal

order to get a stable laser cavity, practice showed that the stability with this calculation should be greater than 0.7, though. The stability range is bigger than 0.5mm and thus not too small. Hence, it is possible to build the laser.

After the ring cavity was built, the distances between the curved mirrors and the crystals

(Ti:Sa, AOFS) were optimized. The calculations of the stability zones showed that the distances between the AOFS and its curved mirrors can be slightly increased without significantly changing the laser stability. Hence, it was possible to change the alignment from a regular ring laser to an FSF laser by only moving the AOFS and tilting its two curved mirrors. Additionally, a Faraday isolator (FI) was inserted into the cavity. Since the two polarizers of the FI only introduced loss, we decided to use the Ti:Sa crystal oriented under Brewster angle as the polarizer. The Brewster angle favors horizontal polarization because the losses for vertical polarization are significantly higher. Hence, the FI was stripped of its polarizers. The so obtained setup can be seen in Figure 3.6.

Unfortunately, due to the low AOFS diffraction efficiency the gain did not suffice to get

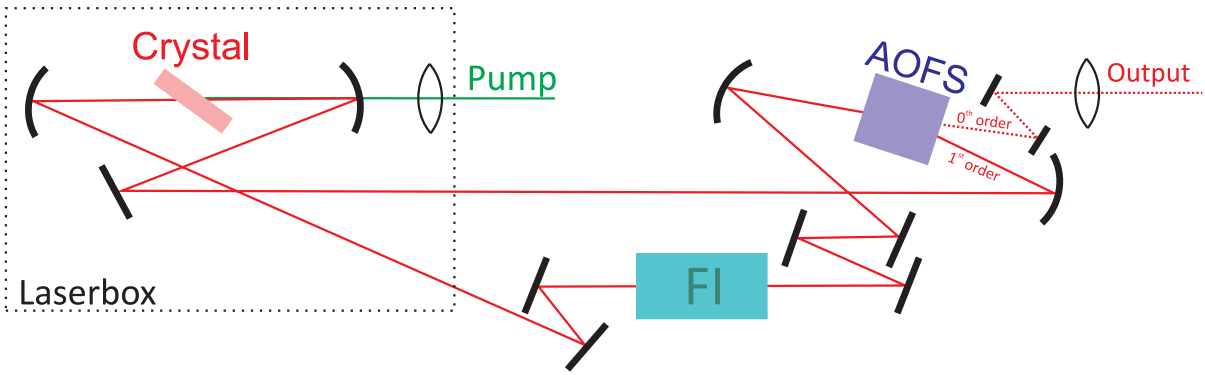

Figure 3.6.: Cavity of the FSF laser

lasing in our early experiments. In order to find ways to increase the gain, the absorption of the Ti:Sa crystal was measured. Therefore, the optical power of the pump light was measured in front of the crystal and after the crystal. The results can be seen in Figure 3.7.

Saturation of the crystal is not yet visible but the 3mm crystal absorbs significantly more

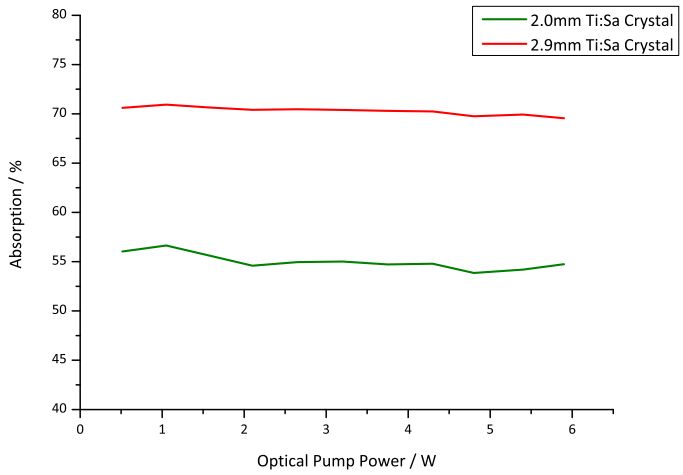

Figure 3.7.: Pump-light absorption of the Ti:Sa crystals

than the 2.0mm crystal. Most Ti:Sa laser oscillators work with an absorption in the order

of 70%. This fact would indicate that the 2.9mm crystal is the preferred choice.
The next interesting quantity is the pump profile in the crystal. To characterize the beam profile, a CCD (Charge-Coupled Device) camera was mounted on a translation stage with micrometer precision. The Ti:Sa crystal was then replaced by the camera which allows measuring the beam profile. The result can be seen in Figure 3.8.

The beam is focused a Gaussian width 2w of about 40μm. It is obviously not possible

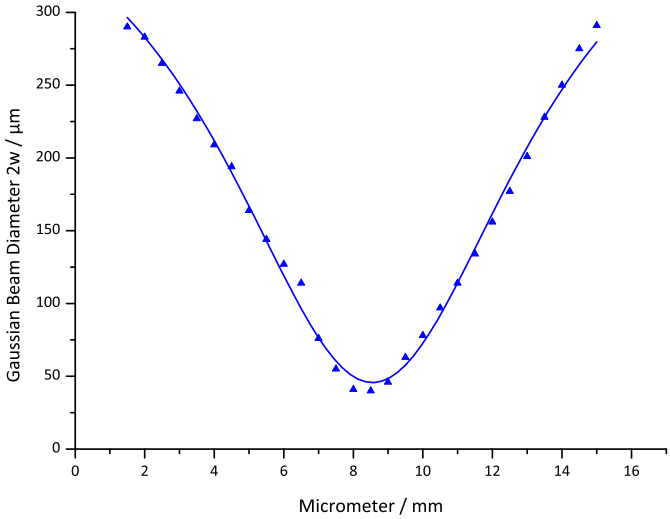

Figure 3.8.: Beam profile of the pump mode at the position of the Ti:Sa crystal

to measure the beam profile of the laser mode, because when measuring in the cavity there would be no lasing. Therefore, one can only numerically calculate the mode size in the crystal. Numerical simulations of the beam profile showed a Gaussian width 2w of about 20μm. The laser box was previously used for a femtosecond-pulse generation and soft-aperture Kerr-lens mode locking requires a bigger the pump mode then would be required for continuous-wave (CW) operation. That means for the CW FSF laser that if the pump mode can be decreased in the crystal, the laser mode would stay the same but would experience more gain. The easiest way to achieve a smaller pump mode is to use bigger pump beam. If the beam is twice as big, the focal spot will be half as big.
Hence, the next step was to build a telescope to increase the pump beam diameter by a factor of two. A concave lens with a focal length of -50mm and a convex lens with a focal length of 100mm were used for the telescope. Since the 2.9mm crystal absorbs more light, it used in the FSF laser. After the new parts were incorporated into the laser, it finally lased.
The output of the FSF laser was collimated with a lens, as shown in Figure 3.6. The collimated beam was then sent to the Michelson interferometer consisting of a beam splitter and two high-reflecting mirrors. One of the mirrors was mounted on a translation stage. A photodiode was placed at the output of the Michelson interferometer and the RF-spectrum was measured.

3.4 Photos of the laser

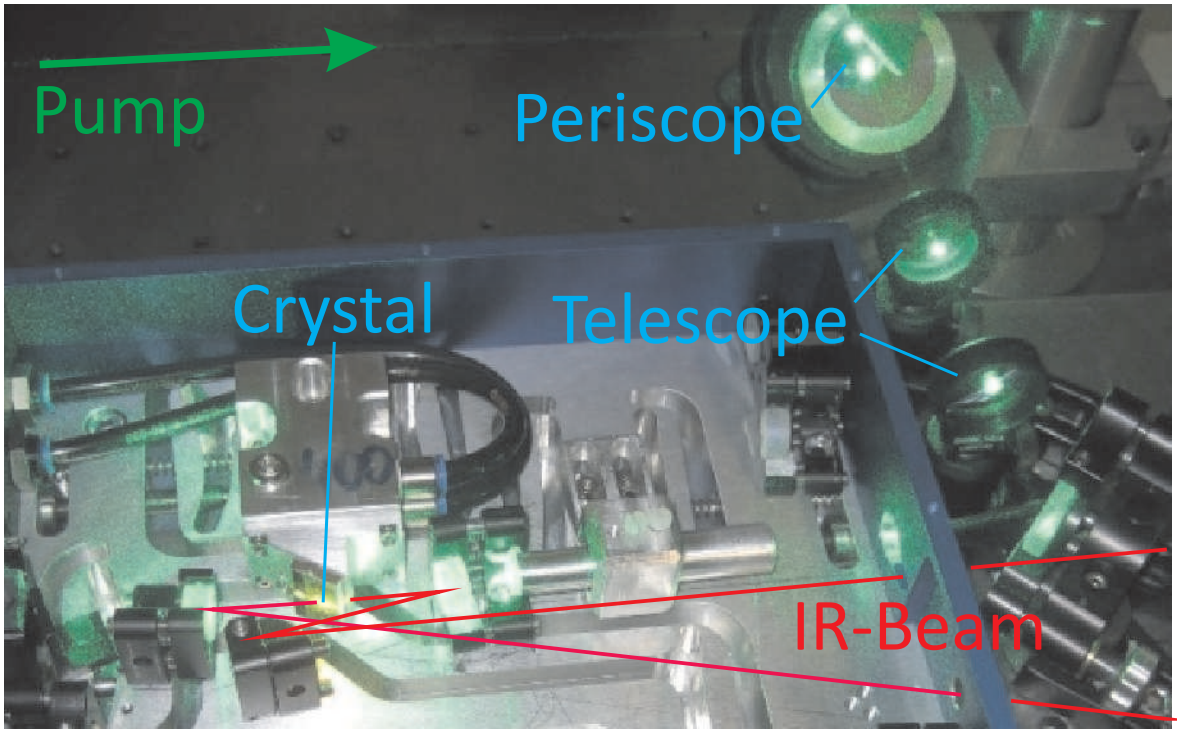

Figure 3.9.: Laser oscillator near the crystal

Figure 3.9 shows the FSF laser near the crystal. The output of the Verdi has to pass a periscope to change the polarization from vertical to horizontal. Afterwards the light passes through the mentioned telescope before it is focused into the crystal. Both curved mirrors which can be seen in Figure 3.9 are transparent for 532nm (pump wavelength) and therefore most of the transmitted pump light is not reflected into the cavity but stays in the laser box where it is absorbed by a beam dump. The infrared beam of the FSF laser leaves the laser box through the hole on the bottom of the picture and come back through the other hole, close to the pump beam.
Outside the laser box, the exiting infrared beam is reflected so that it is parallel to the entering beam and then it enters Figure 3.10 on the left side. First, it passes through the FI before it gets focused into the AOFS. The first-order diffracted beam is reflected back into the laser box and the zeroth-order diffracted beam is collimated with a lens before entering the Michelson interferometer (purple line). The beam splitter (BS) splits the beam. Both beams are reflected with high-reflecting mirror and get combined at the other side of the BS. This combined beam is then directed to the photodiode (PD) where the RF spectrum can be observed.

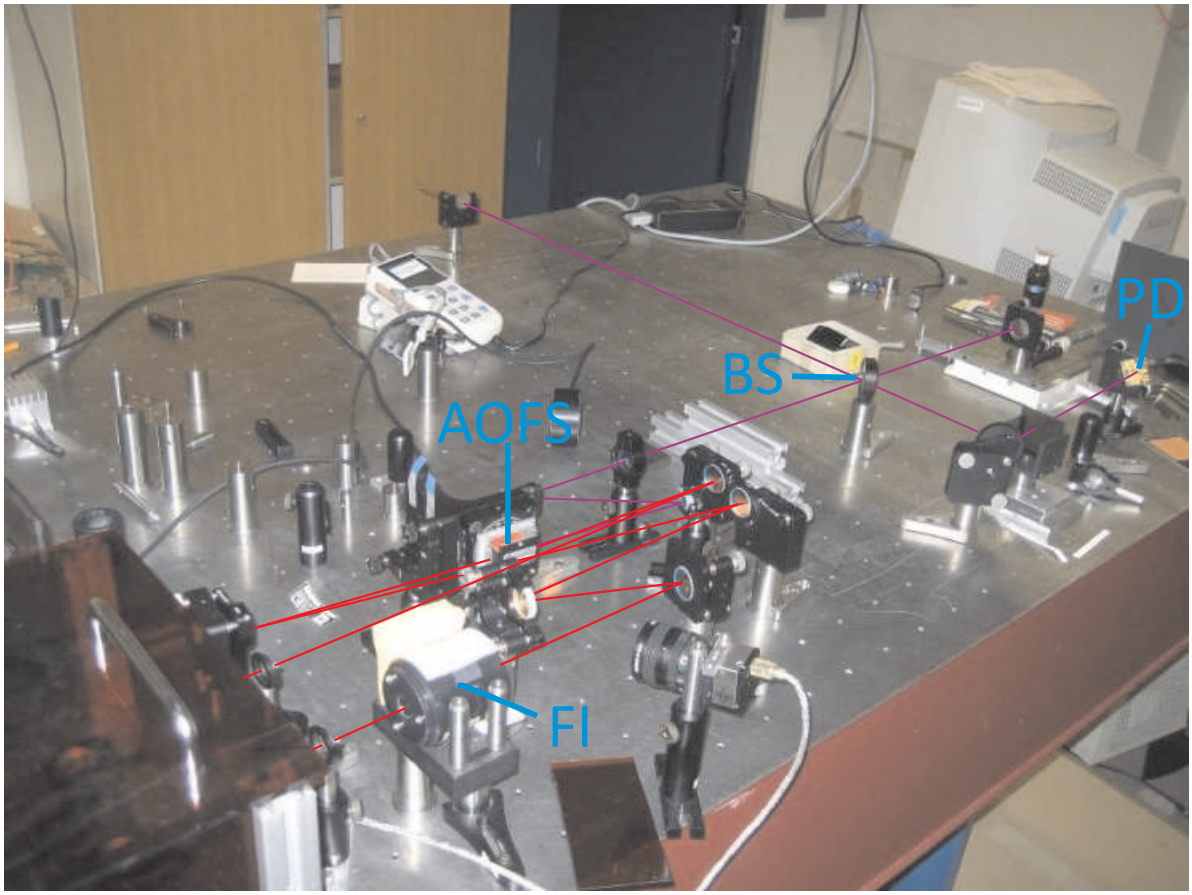

Figure 3.10.: Laser and Michelson interferometer

4 Measurement

This chapter focuses on measuring the optical properties of the laser described in the previous chapter, the RF spectrum with the beat signal, and on measuring distances. Additionally, two laser line filters[1] were inserted into the cavity to force the FSF laser to operate in a narrow wavelength range.

The optical properties of the laser line filters can be seen in Table 4.1. If a laser line

	Transmission	λ_C / **nm**	**FWHM / nm**
Semrock LL01-780-12.5	$> 97\%$	780	3
LOT Oriel LLF785-12.5	$> 97\%$	785	2-3

Table 4.1.: Optical properties of the laser line filters

filter gets tilted, the transmission wavelength will decrease. The longest transmission wavelength is achieved when the beam is perpendicular to the surface of the laser line filter. Hence, the center wavelength of the FSF laser can be tuned by tilting the filter. It is even possible to tilt both filters in a way that lasing is possible with both of them in the cavity.

4.1 Optical properties

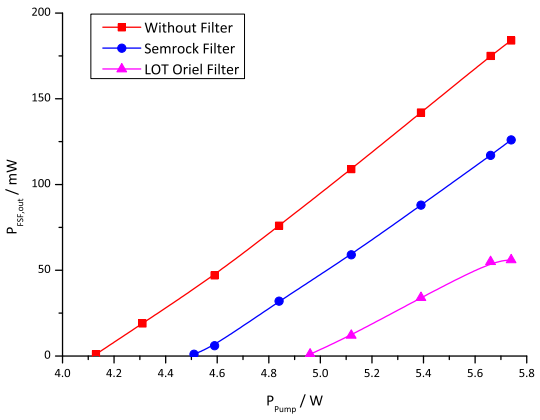

Figure 4.1.: Optical output power in dependence of the pump power for various filters

In Figure 4.1, we can see the dependence of the output power from the pump power. A Coherent Fieldmaster with a LM-10 HTD head was used for the power measurement. The threshold without any filter is obviously the lowest. We can also see that the transmission

[1]Laser line filters are narrow bandpass filters with peak transmission greater than 95%.

of the Semrock Filter is higher than that of the LOT Oriel Filter because the threshold of the Semrock is significantly lower.

In Figure 4.2, we can see the normalized spectra of the FSF laser for various filters. A

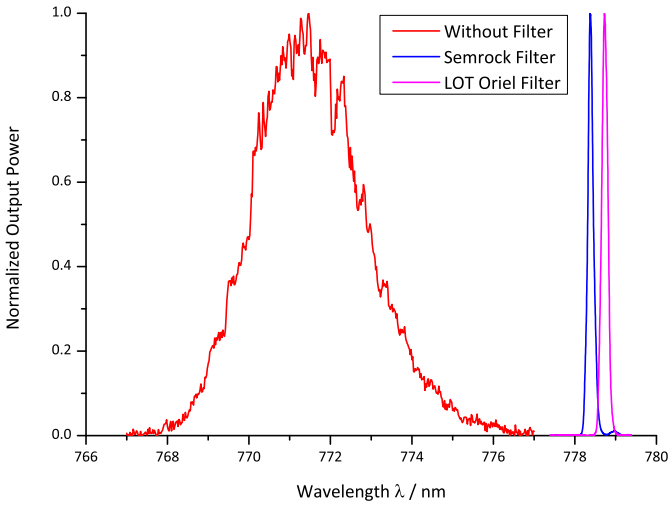

	FWHM / nm
Without Filter	3
Semrock Filter	0.15
LOT Oriel Filter	0.17

Figure 4.2.: Optical spectrum for various filters

Yokogawa AQ-6315A Optical Spectrum Analyzer was used to measure the optical spectrum. Of course, the spectrum without any filter is the broadest. The spectrum without any laser line filter can be shifted by tilting the AOFS because there is a wavelength dependence of the diffraction in the AOFS. So, when the AOFS gets tilted, another wavelength will have optimal alignment in the cavity.
The laser line filters reduce the spectral bandwidth drastically. In the following chapter, we will see what influence this bandwidth reduction has on the measured RF signal.

4.2 Measurement without a laser line filter

Figure 4.3 shows the normalized optical spectrum for various pump powers. The spectra, measured with a resolution of 2pm, are not as smooth as the ones with a laser line filters because without a laser line filter, the losses over the lasing range are similar and the actual output power depends on the spectral gain of the Ti:Sa crystal. The central wavelength shifts slightly to longer wavelengths for higher pump powers. The full width half maximum (FWHM) stays nearly independent of the pump power and is about 3nm. This width is defined by the gain and losses of the cavity. The central wavelength of the peak can be tuned with the AOM because the diffraction angle of the light depends on the wavelength. Hence, when tilting the AOM, another wavelength will be better aligned. In Figure 2.8, the resulting beat frequencies were shown in dependence of the distance. For one fixed distance, the spectrum has peaks every $\frac{1}{T_R}$ and in between two of those

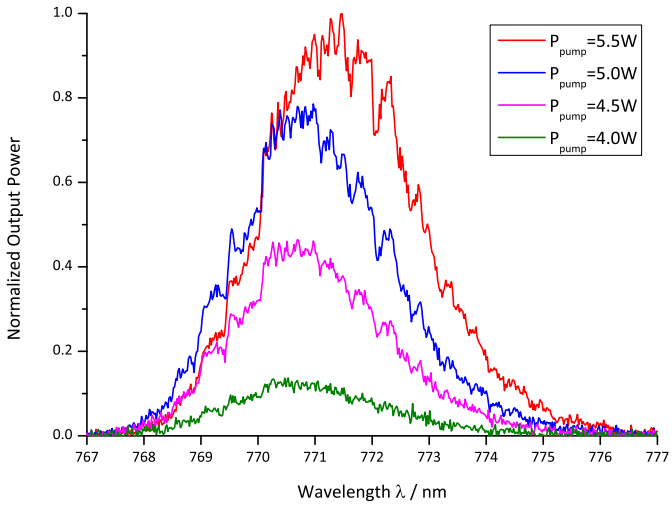

Figure 4.3.: Optical spectrum of the FSF laser without a laser line lilter

peaks, there are two peaks whose positions depend on the distance. The RF spectrum in the laser setup was measured with a photodiode and the *Rohde&Schwarz FSP - Spectrum Analyzer 9kHz ... 30 GHz* (see 4.4). The measured spectrum matches the predicted

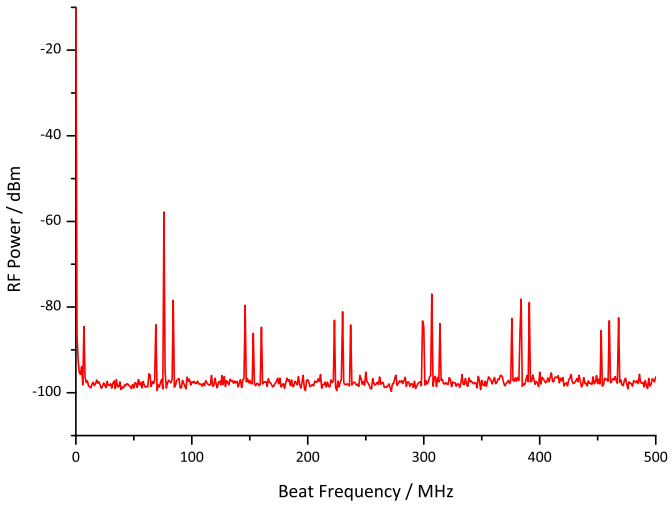

Figure 4.4.: RF spectrum of the beat frequencies of the FSF laser without a laser line filter from 0 to 500MHz

spectrum nicely. The spectrum repeats itself every 75-80MHz. The exact value will be discussed later in this chapter. The peaks that correspond to the repetition rate ($\frac{1}{T_R}$) are always the central peaks in the groups of these three peaks. The other two peaks are the length-dependent beat signals.

Note: The spectrum analyzer has to operate at frequencies greater than 9kHz, and the peak at 0Hz corresponds to the LO feedthrough. Additionally, a DC-blocker with a cut-off

frequency of 10MHz was used. Thus, the absolute spectral value for frequencies below 10MHz is not correct as can be observed in the spectrum. Another important fact is that the noise level of the analyzer depends on the frequency resolution. So, different noise levels do not mean another setup, it is just another frequency resolution in the spectrum analyzer. If the frequency resolution is in the order of the width of the peaks, as in Figure 4.4, the peak height will vary every sweep. With higher resolution, this problem vanishes.

In Chapter 2.3.4, it was discussed to use the frequency range from $\frac{1}{2T_R}$ to $\frac{1}{T_R}$ (= repetition

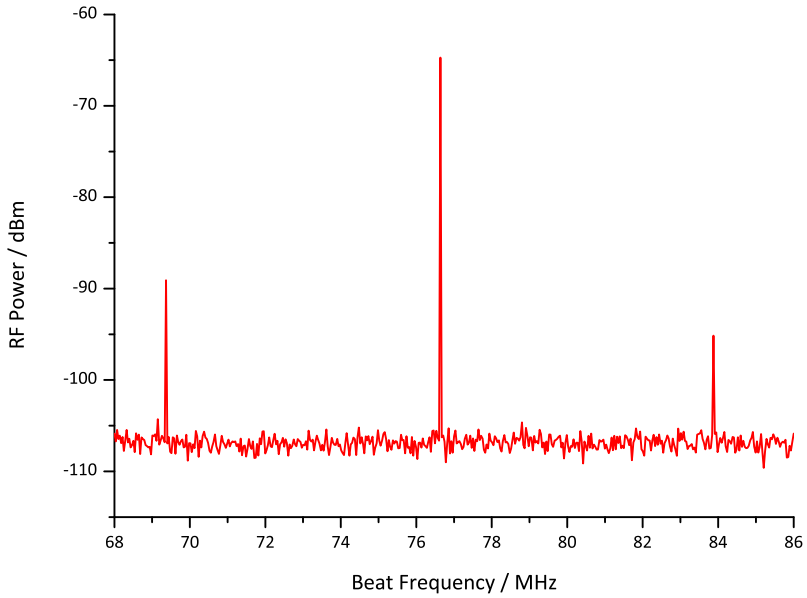

Figure 4.5.: RF spectrum of the beat frequencies of the FSF laser without a laser line filter from 68 to 86MHz

rate). In Figure 4.5, the spectrum near the repetition rate can be seen. The central peak corresponds to the repetition rate. The left peak represents the green or blue line in Figure 2.11 below the repetition rate and shows the length dependence. The right peak also shows the length dependence but it is not in the discussed frequency range.

The peak that represents the repetition rate consists of two different contributions, as can be seen in Figure 4.6. The first has a width of about 30kHz and is 25dB above noise level. The second is a sharp resonance with a width of only a couple of kHz that is 65dB above noise level. Hence, the repetition rate is 76.652MHz and that corresponds to a round-trip time of 13.05ns. The cavity round-trip length

$$L_{opt} = c_0 T_R = 3.911m \tag{4.1}$$

matches the measured length of the resonator of 3.867m (Figure 3.3) nicely, considering different refractive indices in the Ti:Sa crystal, the AOFS and the FI. The repetition rate of about 76MHz implies that frequency steps of about 76kHz are required. With the principle shown in Figure 2.13, a frequency resolution of about 38kHz can be reached

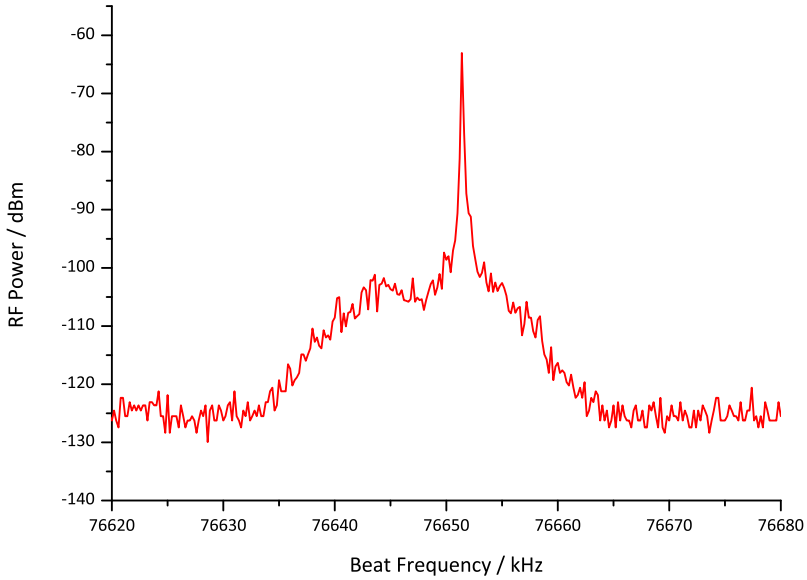

Figure 4.6.: RF spectrum of the peak of the beat frequency corresponding to the repetition rate of the FSF laser without a laser line filter

which corresponds to the desired accuracy of 0.25mm.

The peak that shows the length dependence of Figure 4.7 has a (total) width of about

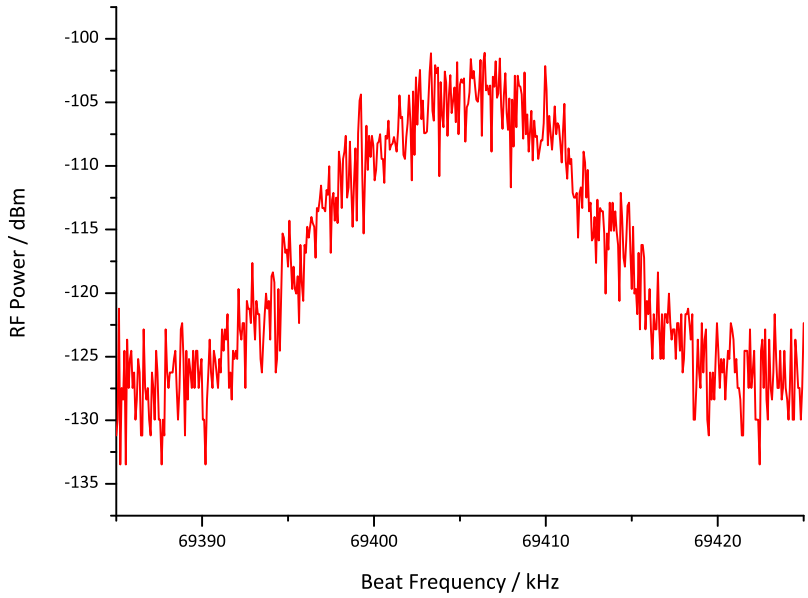

Figure 4.7.: RF spectrum of the length-dependent peak of the beat frequency of the FSF laser without a laser line filter

30kHz and is about 25dB above noise level. Thus, a frequency resolution of 30kHz instead of 38kHz would be possible. The smaller frequency resolution would result in a length

resolution of about 0.2mm. When the micrometer screw was turned slightly, the change in distance was always observed in a shift of the whole peak. The limiting factors for the length resolution are the resolution of the RF spectrum analyzer and the noise on the signal. That implies that it is theoretically possible to measure distances with a higher accuracy. But this will be more time and hardware demanding because each peak has to be resolved with multiple measurements instead of one single measurement.
In the setup, the reference arm had a length L_{ref} of about 77cm and the measurement arm L_m had a length of about 31cm. The length difference $L = L_m - L_{ref}$ is therefore about -46cm. The interferometrically measured length

$$L = -\frac{69.406MHz}{76.652MHz} L' = -0.90547 \frac{2.99792458 \cdot 10^8 m/s}{2 \cdot 300MHz} = -45.24cm \tag{4.2}$$

is obviously more accurate than the measurement with a ruler.

4.2.1 Different pump powers

In this chapter, the influence of the pump power onto the measurement will be discussed.
Figure 4.8 shows the spectra of the beat signals from 0 to 500MHz which do not show

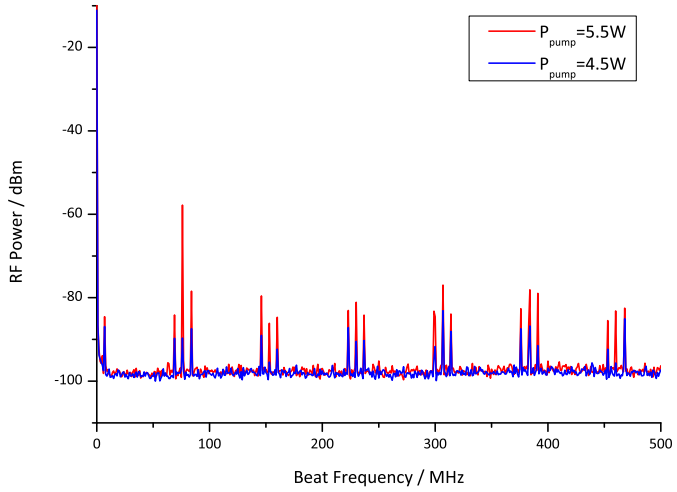

Figure 4.8.: RF spectrum of the beat frequencies of the FSF laser without a laser line filter from 0 to 500MHz for two different pump powers

any significant difference for different pump powers. Because of the lower output power of the FSF laser, the beat signals are obviously weaker in magnitude.
A more detailed analysis of the first group of three peaks shows only a different magnitude but no other influence on the repetition rate peak or the beat signals containing the length dependence, as can be seen in Figure 4.9.

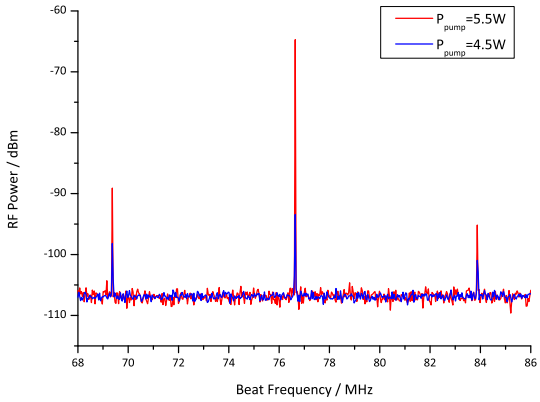

Figure 4.9.: RF spectrum of the beat frequencies of the FSF laser without a laser line filter from 68 to 86MHz for two different pump powers

The length-dependent peak in Figure 4.10 exhibits only a lower magnitude for a lower pump power.

The peak corresponding to the repetition rate in Figure 4.11 shows that, too, but it also

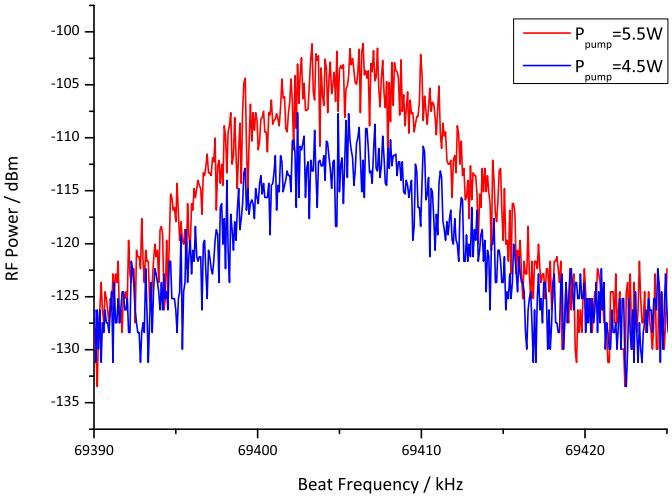

Figure 4.10.: RF spectrum of the length-dependent peak of the beat frequency of the FSF laser without a laser line filter for two different pump powers

shows no sharp resonant peak for the lower pump power. It is at present not yet clear why the resonance vanishes but it might have something to do with the cavity length fluctuations described by Yatsenko *et al.* [18]. In Figure 4 of [18], the influence of the cavity-length fluctuations on the resulting RF signal is shown. For no fluctuations, only a sharp resonance is visible. With increasing fluctuations, a broad noise curve starts consuming the peak until at some point the peak vanishes.

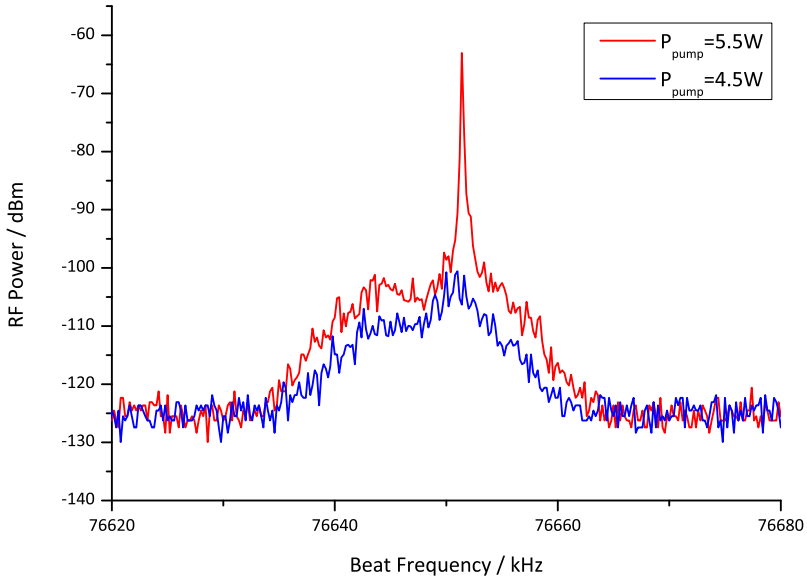

Figure 4.11.: RF spectrum of the peak of the beat frequency corresponding to the repetition rate of the FSF laser without a laser line filter for two different pump powers

4.2.2 Different distances

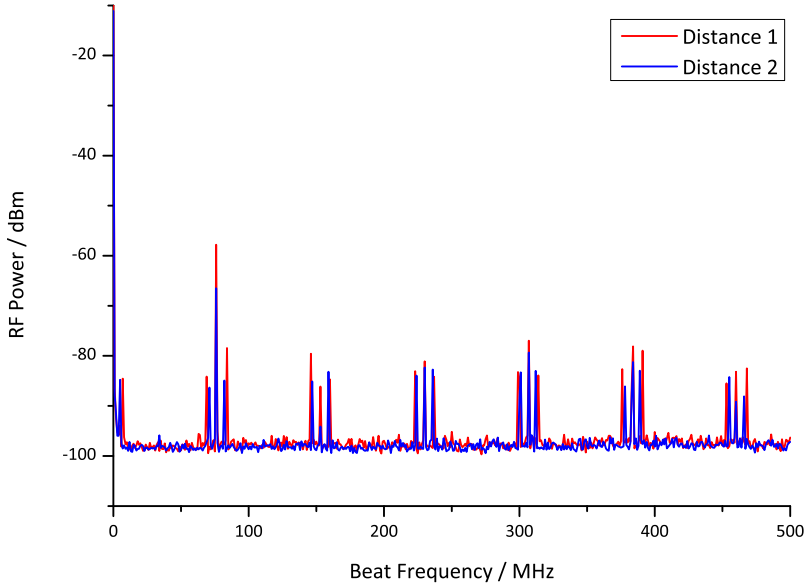

Figure 4.12.: RF spectrum of the beat frequencies of the FSF laser without a laser line filter from 0 to 500MHz for two different distances

One of the mirrors of the Michelson interferometer was mounted on a translation stage. In this chapter, an aluminum plate was put at the end of the table and so it was moved by the thickness of the plate.

Figure 4.12 shows the RF spectrum for the two different lengths. As expected, the repetition rate peaks did not shift but the length-dependent peaks shifted.

Figure 4.13 illustrates this behavior even more explicitly. The central peak is at the same

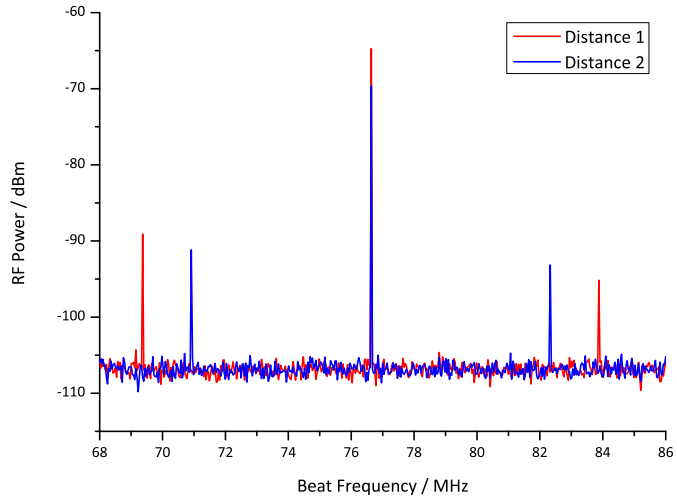

Figure 4.13.: RF spectrum of the beat frequencies of the FSF laser without a laser line filter from 68 to 86MHz for two different distances

position for both distances. But the other two peaks have moved about 0.7MHz closer to the central peak for the second distance. As already mentioned, the different height of the beat signals is due to the measurement process of the RF spectrum analyzer.

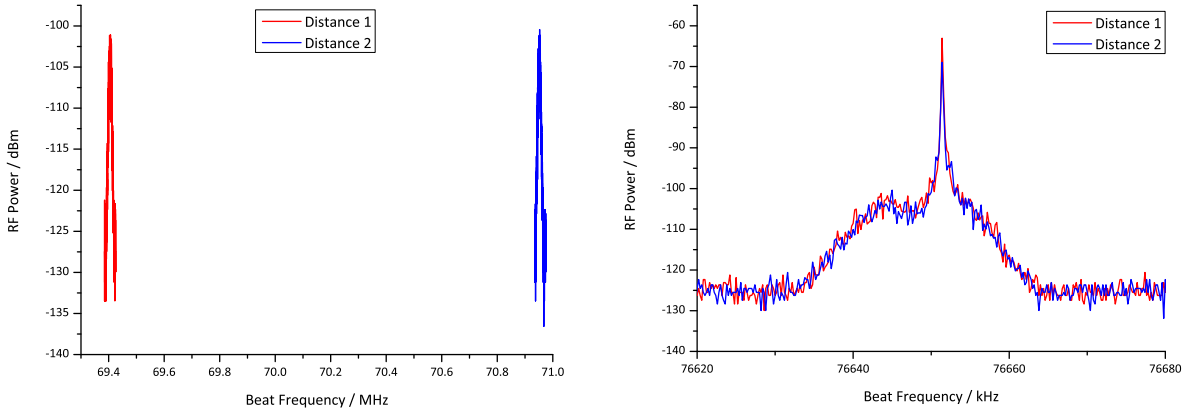

Figure 4.14.: RF spectrum of the beat frequencies of the FSF laser without a laser line filter near the peaks for two different distances. The left panel corresponds to the length-dependent peak and the right to the repetition rate.

A detailed analysis of the RF spectrum of the beat signals can be seen in Figure 4.14. The repetition rate peaks match each other very well. The peaks that exhibit length dependence have similar shape and width. In the following, these peaks are used to measure the thickness of the aluminum plate.
In Chapter 4.1, the length of the first distance was measured to be $L_1 = -45.24cm$. The second peak has a central frequency of 70.952MHz and that results in a length

$$L_2 = -\frac{70.952MHz}{76.652MHz} L' = -0.92564 \frac{2.99792458 \cdot 10^8 m/s}{2 \cdot 300MHz} = -46.25cm \quad . \tag{4.3}$$

The thickness of the aluminum plate is therefore

$$d = L_1 - L_2 = 1.01cm \quad . \tag{4.4}$$

4.3 Reducing the optical bandwidth with a laser line filter

As mentioned in Chapter 2.4 in the discussion of Eq. (2.21), Yatsenko *et al.* [18] showed a dependence of the width of the RF beat signals from the optical bandwidth. The more optical bandwidth, the narrower the RF beat signal will be. Since a spectrally narrow beat signal is desired, a large optical bandwidth seems to be the goal. That is valid for unseeded FSF lasers.
As mentioned in Chapter 2.4, the SNR of the measurement with unseeded FSF laser is very low. If one uses a phase-modulated seed laser, as proposed in [18], the SNR will increase drastically. The disadvantage is that before one can check if a certain frequency exists in the RF spectrum, one has to do a phase modulation on the seed laser with this frequency. Then one has to wait for this light to fill the whole optical spectrum, before the electrical frequency comparison can be made. Thus, the more optical bandwidth one has, the longer one has to wait for the light to fill the whole optical spectrum. That will reduce the frame rate of the desired 3D video.
Since the relation of the optical bandwidth with the RF bandwidth of the beat signals will become important, the following chapters will investigate this relation in the experimental setup.

4.4 Measurement with the Semrock laser line filter

The Semrock Laser Line Filter was inserted into the cavity of the FSF laser. With the filter, the optical spectrum was reduced from 3nm to 0.15nm. Figure 4.15 exhibits the optical spectrum for three different pump powers. The losses in the cavity are dominated by the filter, thus the position of the central wavelength and the FWHM of the optical spectrum do not show a dependence of the pump power. By tilting the filter, its central wavelength can be tuned. This might lead to a bad alignment, as can be seen as the green

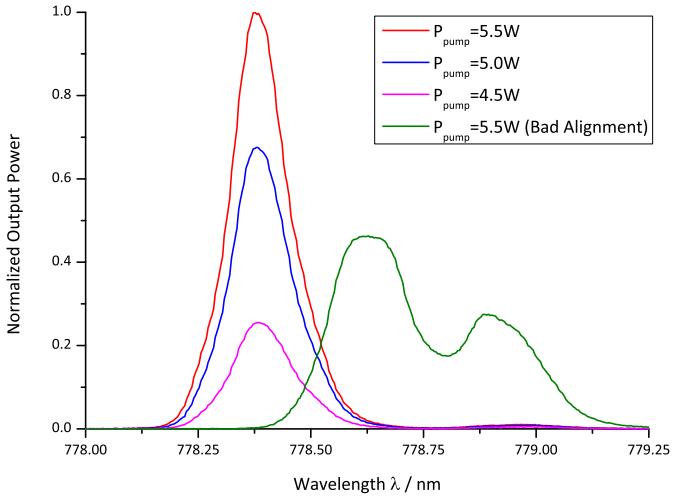

Figure 4.15.: Optical spectrum of the FSF laser with the Semrock laser line filter

line. The implications of such a bad alignment will be discussed in Chapter 4.4.2.

In Figure 4.16, the RF spectrum can be observed. It has its usual shape but the peaks

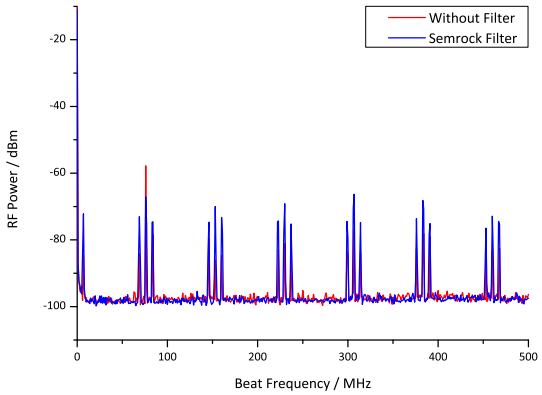

Figure 4.16.: RF spectrum of the beat frequencies of the FSF laser with the Semrock laser line filter from 0 to 500MHz

are broader than those without the filter. This fact is even better illustrated in Figure 4.17, where the repetition rate peak and its neighboring frequencies can be seen. The width of the RF beat signal with a narrow optical bandwidth is significantly bigger than that with a broad optical bandwidth.

Figure 4.18 exhibits a more detailed spectral analysis of the peaks. The width of the repetition rate peak increased to about 2MHz. Since the width without a filter was 30kHz, the width increased by a factor of about 70. The peak that shows the length dependence was also 30kHz and changed to about 2MHz, too. When measuring the distance with the scheme discussed in this thesis, one can either resolve each peak with just one frequency or with multiple frequencies. If one were to resolve with just frequency, the resolution

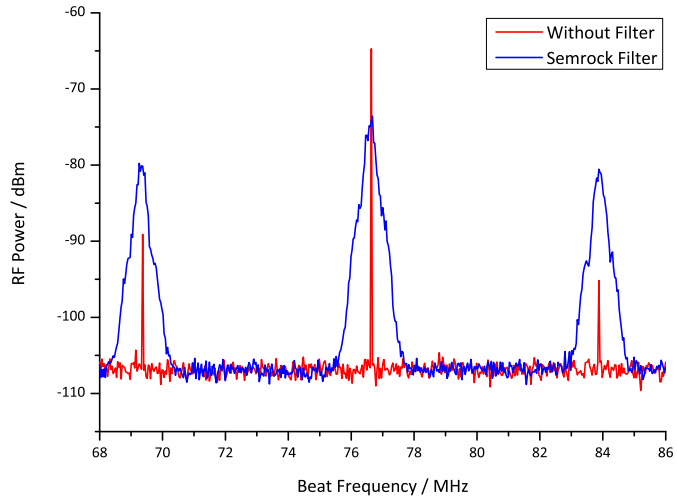

Figure 4.17.: RF spectrum of the beat frequencies of the FSF laser with the Semrock laser line filter from 68 to 86MHz

would reduce with spectrally broad peaks. For example, the increase in RF bandwidth of a factor of 70 would result in a resolution that is 70 times worse and that would correspond to a resolution of about 14mm. If one were to resolve each peak with multiple frequencies, higher resolutions would be possible. But, as already mentioned, it would require more time and more hardware.

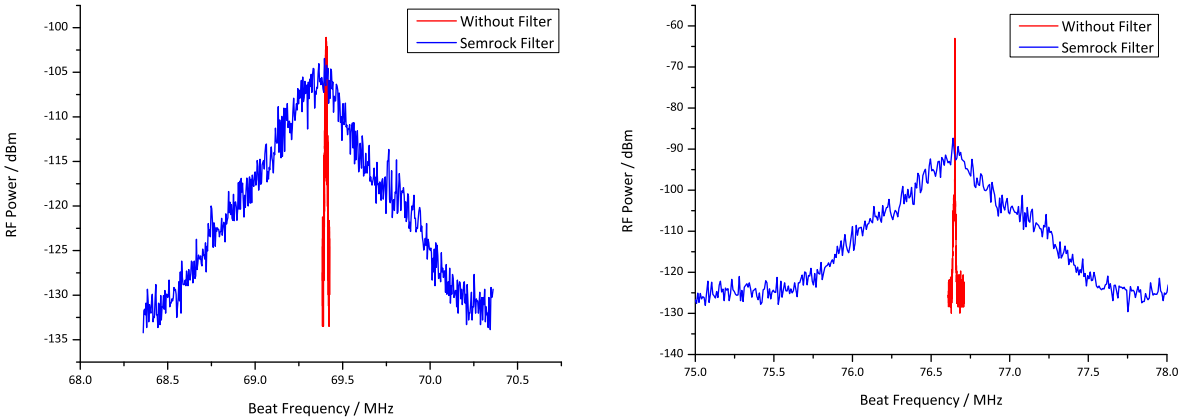

Figure 4.18.: RF spectrum of the beat frequencies of the FSF laser with the Semrock laser line filter near the peaks. The left panel corresponds to the length-dependent peak and the right to the repetition rate.

4.4.1 Different distances

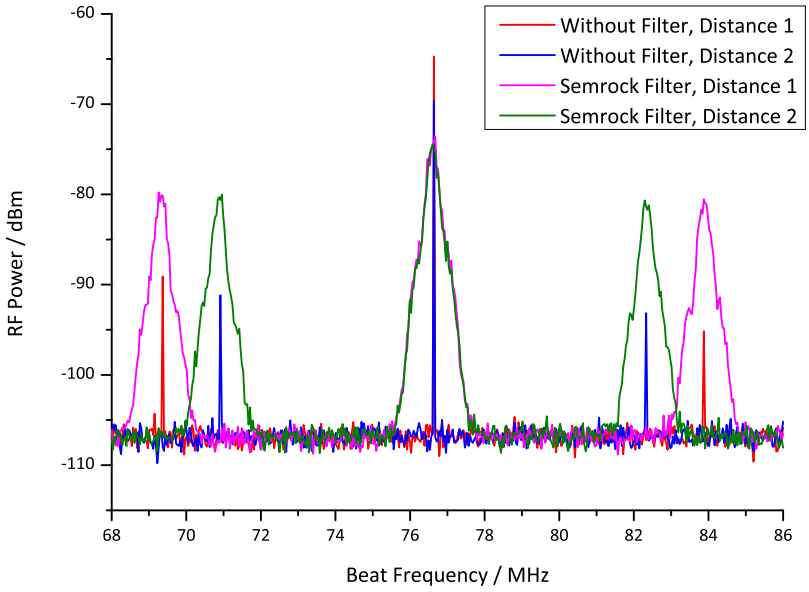

Figure 4.19.: RF spectrum of the beat frequencies of the FSF laser with the Semrock laser line filter from 68 to 86MHz for two different distances

For different distances, the repetition rate peaks stay unchanged. The beat signals with the laser line filter that exhibit the length dependence shifted by the same frequency as the ones without the filter, as can be seen in Figure 4.19 or more clearly in Figure 4.20.

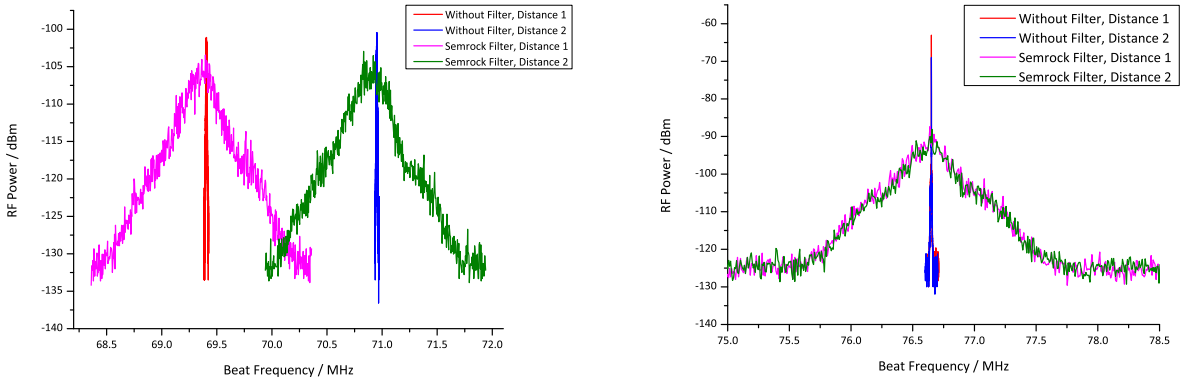

Figure 4.20.: RF spectrum of the beat frequencies of the FSF laser with the Semrock laser line filter near the peaks for two different distances. The left panel corresponds to the length-dependent peak and the right to the repetition rate.

Since the length resolution for resolving with one frequency is about 14mm and the length difference was 10.1cm, the two peaks overlap slightly. Although it is possible to reach a length resolution of about 0.2mm with the last line filter, too, one can easily imagine that the measurement process will be more complicated, more time consuming, and more hardware demanding.

4.4.2 Badly aligned filter

As mentioned before, if the laser line filter is poorly aligned, as can be seen from the green line of Figure 4.15, the optical spectrum can have more than one peak. The implications of such an optical spectrum will be shown in this chapter.

Figure 4.21 exhibits the RF spectrum where each peak contains side peaks. Figure 4.22

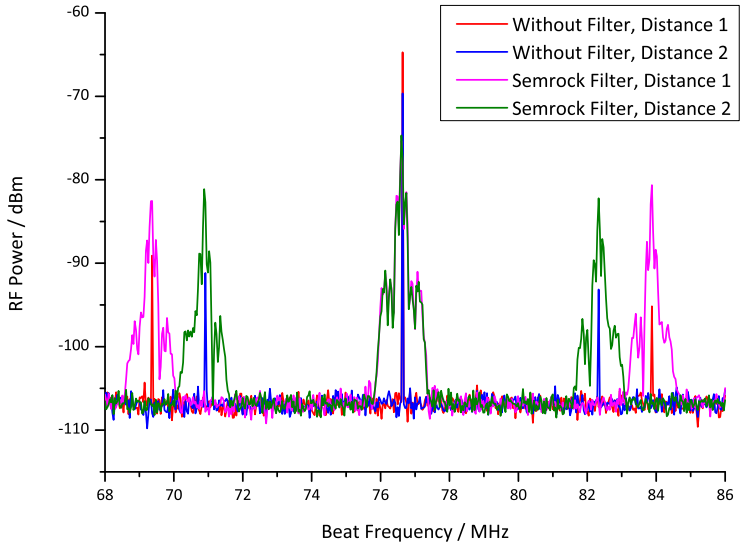

Figure 4.21.: RF spectrum of the beat frequencies of the FSF laser with the badly aligned Semrock laser line filter from 68 to 86MHz for two different distances

shows these side peaks with more detail. It is at the moment not yet clear what causes this RF spectrum. The most likely interpretation of what is happening is that the beat signals of one peak in the optical spectrum interfere with the beat signals of the other peak. This leads to this peculiar RF spectrum.

The side peaks make a detection of the correct frequency more difficult. Hence, it is advisable to work with a nice optical spectrum in order to get an easily interpretable RF spectrum.

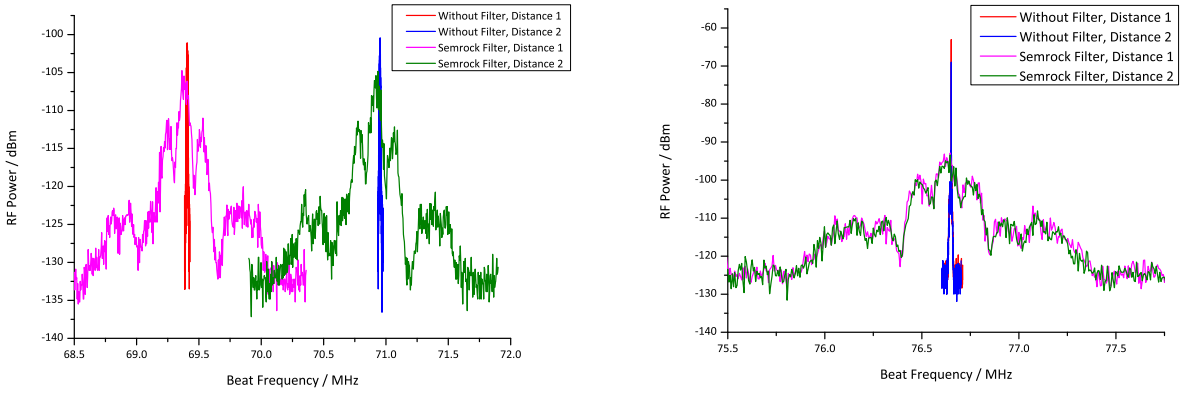

Figure 4.22.: RF spectrum of the beat frequencies of the FSF laser with the badly aligned Semrock laser line filter near the peaks for two different distances. The left panel corresponds to the length-dependent peak and the right to the repetition rate.

4.5 Measurement with the LOT Oriel laser line filter

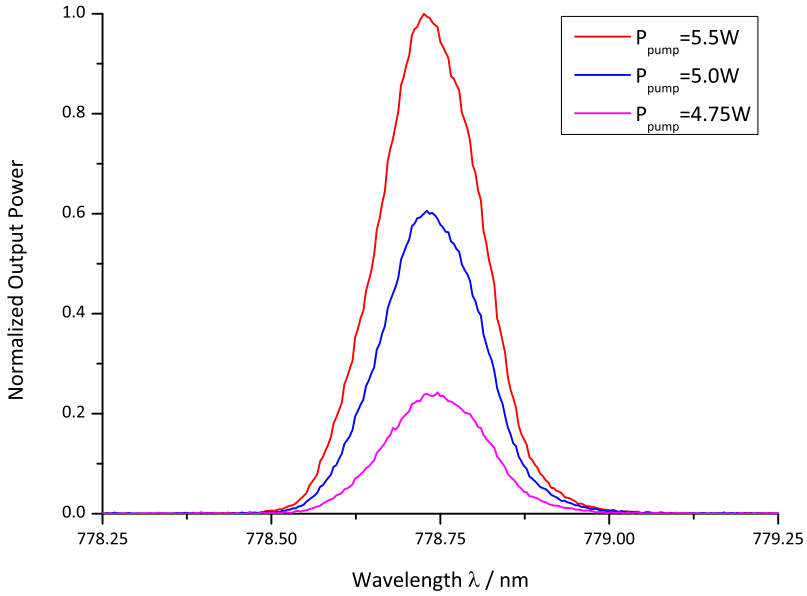

Figure 4.23.: Optical spectrum of the FSF laser with the LOT Oriel laser line filter

The LOT Oriel Laser Line Filter was inserted into the cavity of the FSF laser, and this resulted in an optical bandwidth of 0.17nm. Figure 4.23 shows the optical spectrum for three different pump powers. The losses in the cavity are again dominated by the filter, thus the position of the central wavelength and the FWHM of the optical spectrum do not show a dependence on the pump power. Of course, the central wavelength of the filter can again be tuned by tilting it.

The RF spectrum of Figure 4.24 looks, as was to be expected, very similar to the one

with the Semrock Filter of Figure 4.17. The same is valid for the RF spectrum of Figure 4.24.

A more detailed picture of the peaks, Figure 4.25, exhibits a peak width of about 1MHz

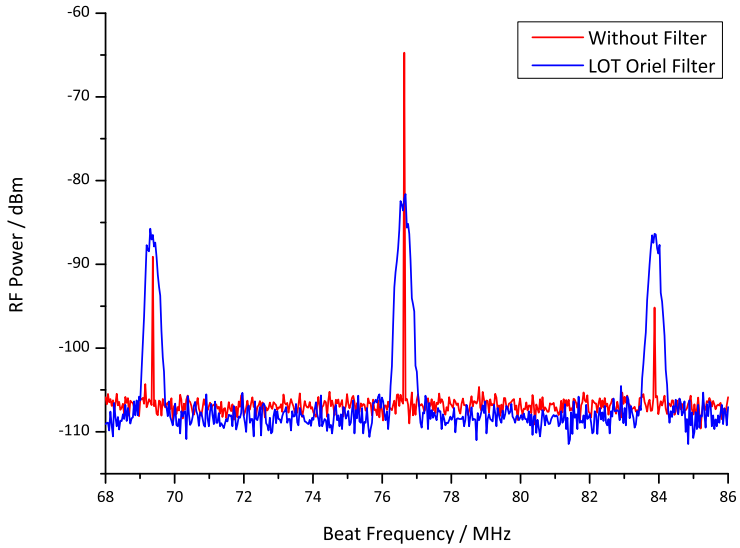

Figure 4.24.: RF spectrum of the beat frequencies of the FSF laser with the LOT Oriel laser line filter from 68 to 86MHz

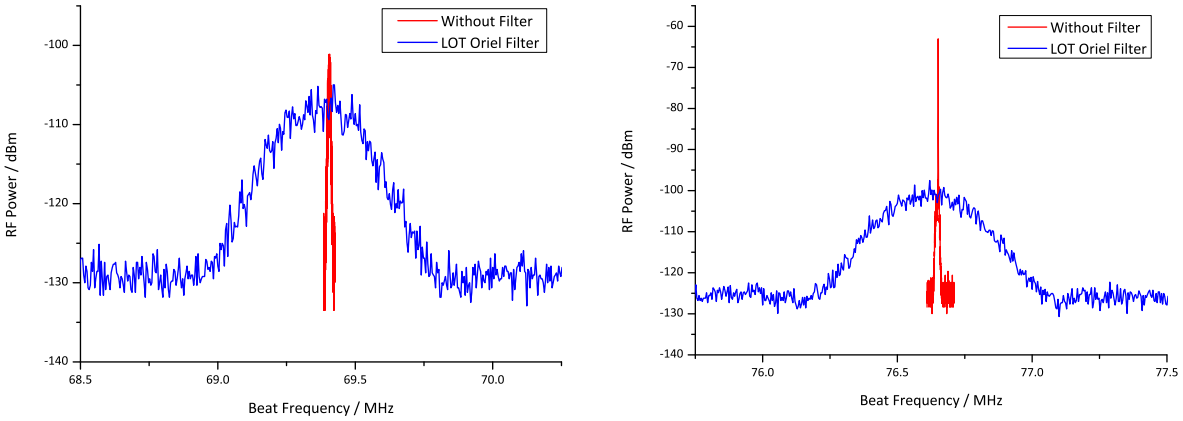

Figure 4.25.: RF spectrum of the beat frequencies of the FSF laser with the LOT Oriel laser line filter near the peaks. The left panel corresponds to the length-dependent peak and the right to the repetition rate.

which is only half of the width observed with the Semrock filter. This is due to a larger optical bandwidth and steeper edges of the optical spectrum. If one chooses to detect only whole peaks, the spectral width of 1MHz would correspond to a length resolution of 7mm. Again, it is still possible to get a better length resolution with more hardware and time demanding measurements.

4.5.1 Different distances

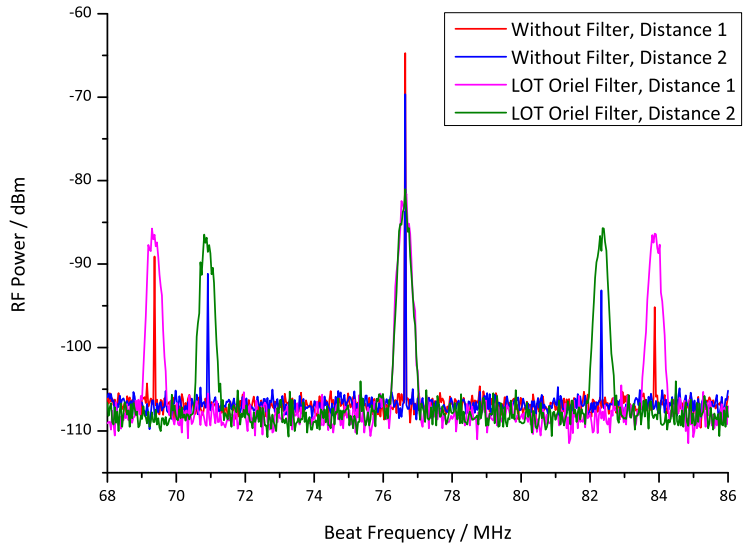

Figure 4.26.: RF spectrum of the beat frequencies of the FSF laser with the LOT Oriel laser line filter from 68 to 86MHz for two different distances

As can be seen in Figure 4.26 and more clearly in Figure 4.27, the two length-dependent peaks do not overlap due to the distance difference of about 10mm and a length resolution of about 7mm.

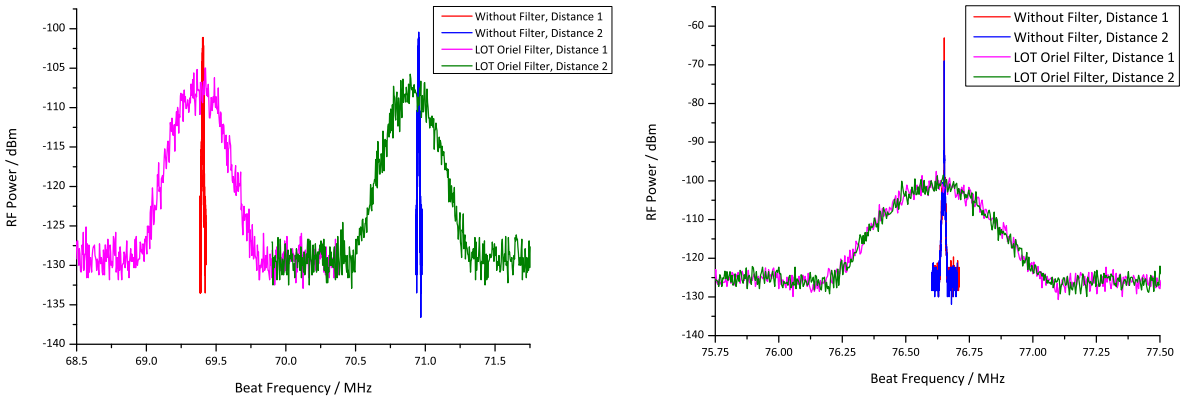

Figure 4.27.: RF spectrum of the beat frequencies of the FSF laser with the LOT Oriel laser line filter near the peaks for two different distances. The left panel corresponds to the length-dependent peak and the right to the repetition rate.

4.6 Measurement with the combination of the Semrock and LOT Oriel laser line filter

Unfortunately, the two laser line filters resulted in similar optical bandwidths of the FSF laser. But it is possible to put both filters in the cavity. They have to be tilted in a way that their transmission bandwidths overlap. At some point, the overlap of the filters will produce the broadest spectrum. If one then increases the tilt angle of the filters, the optical bandwidth will start to decrease. Hence, it will be possible to tune the optical bandwidth (in a certain range). This is shown in this chapter.

Figure 4.28 shows the optical spectrum of two combinations. Combination 2 shows an

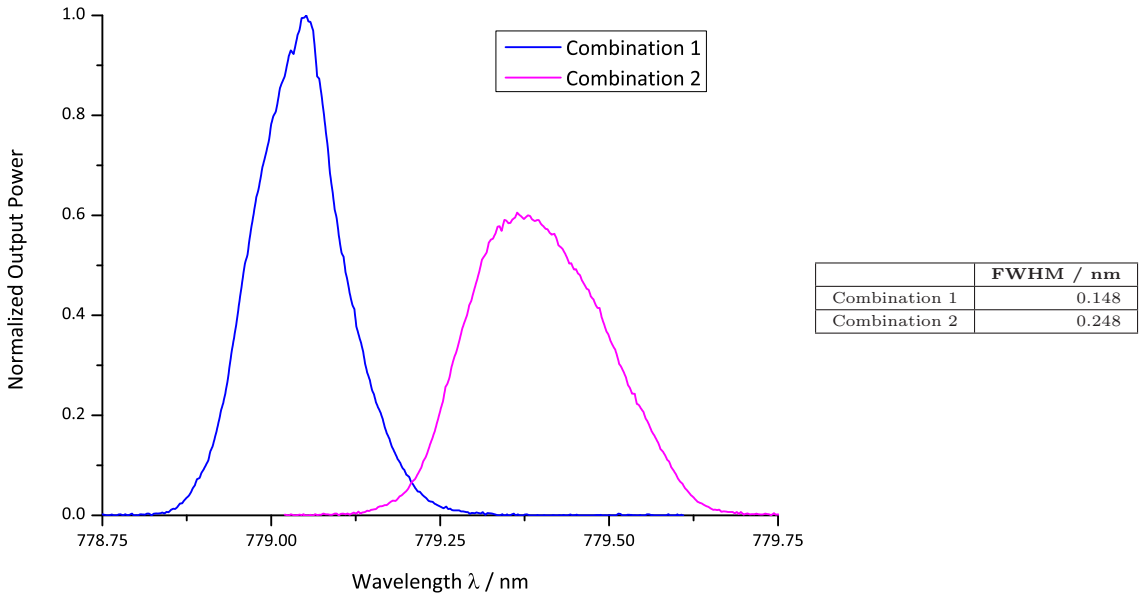

	FWHM / nm
Combination 1	0.148
Combination 2	0.248

Figure 4.28.: Optical spectrum of the FSF laser with a combination of the Semrock and the LOT Oriel laser line filter

optical spectrum that is broader than that of each single laser line filter. That is due to the transmission of the combination of both filters which is broader in this case.

Figure 4.29 shows exactly what had to be expected. If the optical spectrum is broader, the RF spectrum will be smaller. Therefore the RF spectrum of Combination 1 is the broadest and the spectrum of Combination 2 is significantly narrower.

In order to estimate the length resolution for the two combinations, one needs more detailed graphs of the RF spectrum, such as the one in Figure 4.30. The peaks of Combination 1 have a width of nearly 2MHz which would result in a length resolution of about 14mm. Combination 2 has narrower peaks of about 0.4MHz width. This would correspond to a length resolution of 2.8mm.

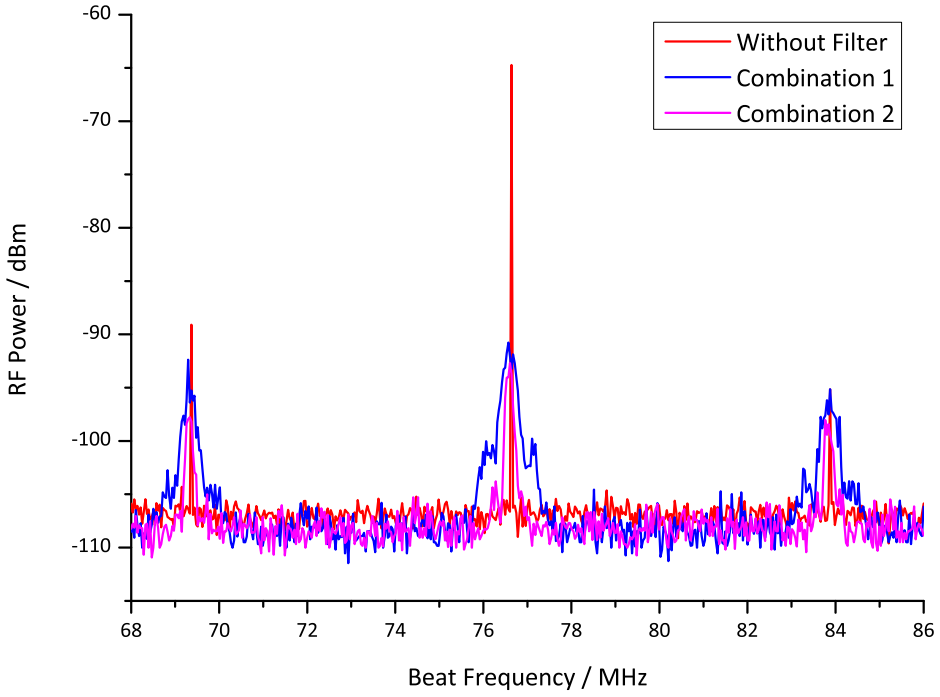

Figure 4.29.: RF spectrum of the beat frequencies of the FSF laser for two combinations of the Semrock and the LOT Oriel laser line filter from 68 to 86MHz

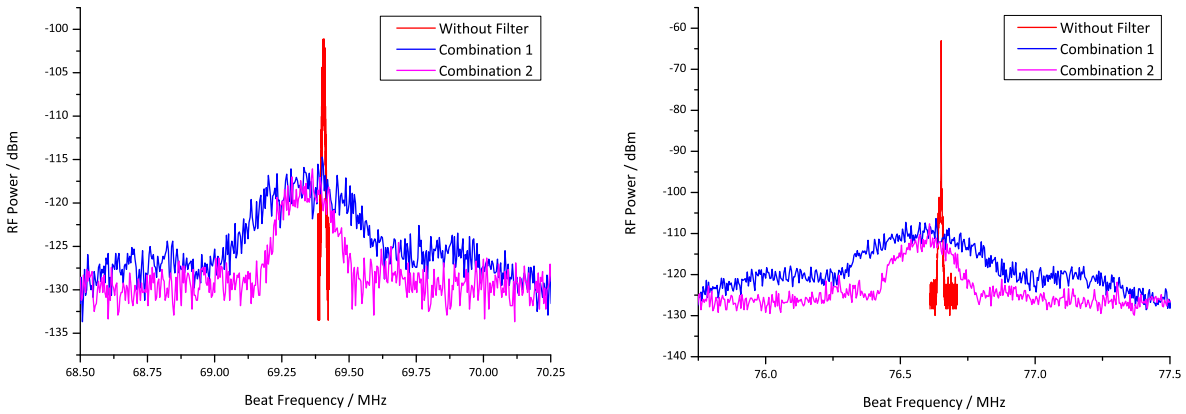

Figure 4.30.: RF spectrum of the beat frequencies of the FSF laser for two combinations of the Semrock and the LOT Oriel laser line filter near the peaks. The left panel corresponds to the length-dependent peak and the right to the repetition rate.

5 Summary and Outlook

The theory of the Moving Comb Model proved to be a very useful tool for calculating the resulting beat frequencies. Its graphical solution provides a very intuitive way to describe the underlying physics. With this model, the ambiguity of OFDR becomes obvious. Changing the AOFS frequency provides a useful tool to get rid of the ambiguity. One of the big advantages of OFDR is that the length resolution is independent of the length which is measured. That means if the length resolution is 0.25mm, it will stay 0.25mm, no matter if 1m or 10km are measured. The mathematical solution allows calculating the distance from the resulting beat frequencies easily.
One problem remains, though. The more accurately a distance is measured, the longer it will take and the less it is allowed to move during the measurement process. Hence, a more precise measurement will allow only very slow moving objects to be detected. For example, increasing the precision by a factor of 2 requires twice as many frequency comparisons and will therefore take twice as long. It will also mean the distance that is changed can only change half as much during one measurement process. Thus, the maximum velocity of an object that can be detected will drop by a factor of 4. One has to find a compromise between accuracy and what moving objects to detect.
The laser in this thesis used an AOM with a frequency of 300MHz. Since the attenuation of an acoustic wave in tellurium dioxide increases exponentially with the frequency, lower AOM frequencies are better for laser with smaller gain. But smaller AOM frequencies increase the unambiguous range. Hence, the unambiguous range has to be divided into more frequency bands in order to get the same length resolution. The measurement of more frequencies takes longer and therefore a lower AOM frequency not only requires more precise hardware due to the narrower frequency bands, but it will also cause the whole measurement cycle to take longer. That results in a lower frame rate. Hence, the solution for future developments should be a laser with higher gain so that AOMs with high frequencies can be used.
The measurements without a laser line filter showed a resolution of 0.2mm when each peak in the RF spectrum was resolved with only one test frequency. That was below the goal of 0.25mm. Unfortunately, the SNR of this measurement principle was very poor. The measurement only worked with mirrors but not with a sheet of paper. To solve this problem, one can use a phase-modulated seed laser as proposed by Yatsenko *et al.* [18]. This scheme requires creating the phase-modulated light according to the frequency that shall be detected. After creation one has to wait for the light with the phase-modulation frequency to fill up the whole spectrum before one can start the electronic measurement of the frequency. Hence, the broader the spectrum is the longer one will have to wait and thus the lower the frame rate of the measurement will be.
That was the reason why measurements with laser line filters were done in order to reduce

the optical bandwidth. The measurement showed broader peaks in the RF spectrum as predicted by Yatsenko *et al.* In order to get the same length resolution, the broader peaks will require a more time-consuming and hardware-demanding measurement. But with the seed laser, the bandwidth of the peaks should decrease due to the smaller bandwidth of the seed laser. Then it should be possible to reach a resolution of 0.25mm with an optical bandwidth of less than 1nm.

A Appendix

A.1 The moving comb model

This section treats the moving comb model that was introduced in Chapter 2.3.

A.1.1 Ring cavity

At first we want to start again with the definitions:

Chirp rate: $$\sigma = \frac{f_{AOM}}{T_R} \tag{A.1}$$

Phase of mode q: $$\varphi_q(t) = \frac{c_0}{\lambda}\left(t - \frac{q}{f_{AOM}}\right) + \frac{\sigma}{2}\left(t - \frac{q}{f_{AOM}}\right)^2 + \phi_q \tag{A.2}$$

Frequency of mode q: $$f_q(t) = \frac{d\varphi_q(t)}{dt} = \frac{c_0}{\lambda} + \sigma\left(t - \frac{q}{f_{AOM}}\right) \tag{A.3}$$

Electric field: $$E(t) = \sum_{q=1}^{N} E_q(t)\ e^{i\,2\pi\varphi_q(t)} \qquad E_q(t) \in \Re \tag{A.4}$$

Intensity: $$I(t) = \frac{nc_0\epsilon_0}{2}\left|E(t)\right|^2 \tag{A.5}$$

We can calculate the intensity after the Michelson interferometer with the two dampings δ and η of the two arms as follows:

$$\begin{aligned} I(t) \propto I_1(t) + I_2(t) + I_3(t) &= \left|\delta\, E(t) + \eta\, E\left(t - \frac{2L}{c_0}\right)\right|^2 \\ &= \delta^2\left|E(t)\right|^2 + \delta\eta\ \left(E^*(t)\ E\left(t - \frac{2L}{c_0}\right) + E(t)\ E^*\left(t - \frac{2L}{c_0}\right)\right) + \eta^2\ \left|E\left(t - \frac{2L}{c_0}\right)\right|^2 \end{aligned} \tag{A.6}$$

$$I_1(t) = \delta^2\left|E(t)\right|^2 \tag{A.7}$$

$$I_2(t) = \delta\eta\ \left(E^*(t)\ E\left(t - \frac{2L}{c_0}\right) + E(t)\ E^*\left(t - \frac{2L}{c_0}\right)\right) \tag{A.8}$$

$$I_3(t) = \eta^2\ \left|E\left(t - \frac{2L}{c_0}\right)\right|^2 \tag{A.9}$$

In the following calculation, we will always encounter products of sums from Eq. (A.4). Let us first define a substitution:

$$\mathcal{E}_i = E_i(t)\ e^{i\,2\pi\varphi_i(t)} \tag{A.10}$$

Since there are only discrete frequencies present, the result will only contain discrete beat frequencies. We can define a beat index p. It states which terms have to be multiplied.

If $p = 0$, only terms with the same index will be multiplied. If $p = 1$, only terms with a difference of one in their index will be multiplied, and so on. This scheme can be seen in Table A.1. Of course, negative values for p are also possible, when the index of the left

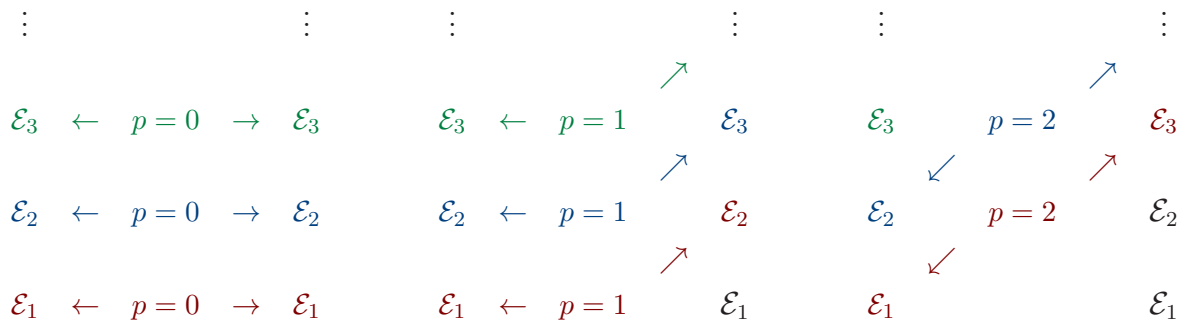

Table A.1.: Pattern for calculating the product of a sum with a sum

column is bigger than that of the right column. In Eq. (A.4) we can see that there are N round-trips in the cavity. Hence, N beat signals will exist. In the autocorrelations of terms $I_1(t)$ and $I_3(t)$, the beat index p fulfills the following inequality, $0 \leq p \leq N-1$. In the term $I_2(t)$, we will encounter a length dependence. This length dependence will cause different beat index values. The number of beat indices does not change, but for example they could start at $-N/2$ instead of 0.
In the following, we will apply this scheme to the three terms.

A.1.1.1 Term $I_1(t)$

$$
\begin{aligned}
I_1(t) = \delta^2 \left|E\left(t\right)\right|^2 &= \delta^2 \left(\sum_{q=1}^{N} E_q\left(t\right)\ e^{i\,2\pi\varphi_q(t)}\right)\left(\sum_{q=1}^{N} E_q\left(t\right)\ e^{-i\,2\pi\varphi_q(t)}\right) \\
&= \delta^2 \sum_{p=0}^{N-1} \frac{1}{2}\Big(E_1\left(t\right)\ E_{1+p}\left(t\right)\ e^{i\,2\pi(\varphi_1(t)-\varphi_{1+p}(t))} + \cdots + E_{N-p}\left(t\right)\ E_N\left(t\right)\ e^{i\,2\pi\left(\varphi_{N-p}(t)-\varphi_N(t)\right)} \\
&\quad + E_{1+p}\left(t\right)\ E_1\left(t\right)\ e^{i\,2\pi(\varphi_{1+p}(t)-\varphi_1(t))} + \cdots + E_N\left(t\right)\ E_{N-p}\left(t\right)\ e^{i\,2\pi\left(\varphi_N(t)-\varphi_{N-p}(t)\right)}\Big) \\
&= \delta^2 \sum_{p=0}^{N-1} \sum_{q=1}^{N-p} \frac{E_q\left(t\right)\ E_{q+p}\left(t\right)\ e^{i\,2\pi(\varphi_q(t)-\varphi_{q+p}(t))} + E_{q+p}\left(t\right)\ E_q\left(t\right)\ e^{i\,2\pi(\varphi_{q+p}(t)-\varphi_q(t))}}{2} \\
&= \delta^2 \sum_{p=0}^{N-1} \sum_{q=1}^{N-p} E_q\left(t\right)\ E_{q+p}\left(t\right)\ \cos\left(2\pi\left(\varphi_q\left(t\right)-\varphi_{q+p}\left(t\right)\right)\right)
\end{aligned}
\tag{A.11}
$$

We can see that the first term can be decomposed into cosines. The higher the beat index, the fewer modes interfere and therefore the weaker the beat signal will be (neglecting amplitude dependence). In the following, we will have a closer look at the phase term $\varphi_q\left(t\right) - \varphi_{q+p}\left(t\right)$.

$$\begin{aligned}\varphi_q(t) - \varphi_{q+p}(t) &= \frac{c_0}{\lambda}\left(t - \frac{q}{f_{AOM}}\right) + \frac{\sigma}{2}\left(t - \frac{q}{f_{AOM}}\right)^2 + \phi_q \\ &\quad - \frac{c_0}{\lambda}\left(t - \frac{q+p}{f_{AOM}}\right) - \frac{\sigma}{2}\left(t - \frac{q+p}{f_{AOM}}\right)^2 - \phi_{q+p} \\ &= \frac{\sigma}{2}\left(\left(t^2 - 2\,\frac{q}{f_{AOM}}\,t + \frac{q^2}{f_{AOM}^2}\right) - \left(t^2 - 2\,\frac{q+p}{f_{AOM}}\,t + \frac{q^2+2qp+p^2}{f_{AOM}^2}\right)\right) \\ &\quad + \frac{c_0}{\lambda}\,\frac{p}{f_{AOM}} + \phi_q - \phi_{q+p} \\ &= \sigma\,\frac{p}{f_{AOM}}\,t - \frac{\sigma}{2}\,\frac{2qp+p^2}{f_{AOM}^2} + \frac{c_0}{\lambda}\,\frac{p}{f_{AOM}} + \phi_q - \phi_{q+p} \end{aligned} \tag{A.12}$$

$$f_{beat,1}(q,p) = \sigma\,\frac{p}{f_{AOM}} = \frac{p}{T_R} \tag{A.13}$$

$$\varphi_{beat,1}(q,p) = \frac{c_0}{\lambda}\,\frac{p}{f_{AOM}} - \frac{\sigma}{2}\,\frac{2qp+p^2}{f_{AOM}^2} + \phi_q - \phi_{q+p} \tag{A.14}$$

A.1.1.2 Term $I_2(t)$

We will use the pattern from the previous chapter to calculate the second term. As already mentioned, the values of the beat index p depend on L. Overall there have to be N terms. If we use $0 \le p \le N-1$, that will corresponds to $0 \le L \le c_0/(2\,f_{AOM})$.

$$\begin{aligned} I_2(t) &= \delta\eta\,\left(E^*(t)\;E\left(t - \frac{2L}{c_0}\right) + E(t)\;E^*\left(t - \frac{2L}{c_0}\right)\right) \\ &= 2\delta\eta\,\sum_{p=0}^{N-1}\sum_{q=1}^{N-p}\frac{E_q(t)\;E_{q+p}\left(t-\frac{2L}{c_0}\right)\;e^{2\pi\left(\varphi_q(t) - \varphi_{q+p}\left(t-\frac{2L}{c_0}\right)\right)}}{4} \\ &\quad + 2\delta\eta\,\sum_{p=0}^{N-1}\sum_{q=1}^{N-p}\frac{E_{q+p}(t)\;E_q\left(t-\frac{2L}{c_0}\right)\;e^{2\pi\left(\varphi_{q+p}(t) - \varphi_q\left(t-\frac{2L}{c_0}\right)\right)}}{4} \\ &\quad + 2\delta\eta\,\sum_{p=0}^{N-1}\sum_{q=1}^{N-p}\frac{E_q\left(t-\frac{2L}{c_0}\right)\;E_{q+p}(t)\;e^{2\pi\left(\varphi_q\left(t-\frac{2L}{c_0}\right) - \varphi_{q+p}(t)\right)}}{4} \\ &\quad + 2\delta\eta\,\sum_{p=0}^{N-1}\sum_{q=1}^{N-p}\frac{E_{q+p}\left(t-\frac{2L}{c_0}\right)\;E_q(t)\;e^{2\pi\left(\varphi_{q+p}\left(t-\frac{2L}{c_0}\right) - \varphi_q(t)\right)}}{4} \end{aligned} \tag{A.15}$$

$$\begin{aligned} I_2(t) &= \delta\eta\,\sum_{p=0}^{N-1}\sum_{q=1}^{N-p}E_q(t)\;E_{q+p}\left(t-\frac{2L}{c_0}\right)\;\cos\left(2\pi\left(\varphi_q(t) - \varphi_{q+p}\left(t-\frac{2L}{c_0}\right)\right)\right) \\ &\quad + \sum_{p=0}^{N-1}\sum_{q=1}^{N-p}E_{q+p}(t)\;E_q\left(t-\frac{2L}{c_0}\right)\;\cos\left(2\pi\left(\varphi_{q+p}(t) - \varphi_q\left(t-\frac{2L}{c_0}\right)\right)\right) \end{aligned} \tag{A.16}$$

This term can be decomposed into two cosines. We will investigate their phases in more detail in the following.

$$\begin{aligned}\varphi_q(t) - \varphi_{q+p}\left(t - \frac{2L}{c_0}\right) &= \frac{c_0}{\lambda}\left(t - \frac{q}{f_{AOM}}\right) + \frac{\sigma}{2}\left(t - \frac{q}{f_{AOM}}\right)^2 + \phi_q \\ &\quad - \frac{c_0}{\lambda}\left(t - \frac{2L}{c_0} - \frac{q+p}{f_{AOM}}\right) - \frac{\sigma}{2}\left(t - \frac{2L}{c_0} - \frac{q+p}{f_{AOM}}\right)^2 - \phi_{q+p} \\ &= \frac{\sigma}{2}\left(\left(t^2 - 2\,\frac{q}{f_{AOM}}\,t + \frac{q^2}{f_{AOM}^2}\right) - \left(t^2 + \left(\frac{2L}{c_0}\right)^2 + \frac{q^2+2qp+p^2}{f_{AOM}^2}\right.\right. \\ &\quad \left.\left. + \frac{4L}{c_0}\,\frac{q+p}{f_{AOM}} - 2\,\frac{q+p}{f_{AOM}}\,t - \frac{4L}{c_0}\,t\right)\right) + \frac{2L}{\lambda} + \frac{c_0}{\lambda}\,\frac{p}{f_{AOM}} + \phi_q - \phi_{q+p} \\ &= \sigma\left(\frac{p}{f_{AOM}} + \frac{2L}{c_0}\right)t - \frac{\sigma}{2}\left(\left(\frac{2L}{c_0}\right)^2 + \frac{4L}{c_0}\,\frac{q+p}{f_{AOM}} + \frac{2qp+p^2}{f_{AOM}^2}\right) \\ &\quad + \frac{2L}{\lambda} + \frac{c_0}{\lambda}\,\frac{p}{f_{AOM}} + \phi_q - \phi_{q+p} \end{aligned} \tag{A.17}$$

$$f_{beat,2a}(q,p) = \sigma\left(\frac{p}{f_{AOM}} + \frac{2L}{c_0}\right) = \frac{1}{T_R}\left(p + \frac{2\,f_{AOM}}{c_0}\,L\right) \tag{A.18}$$

$$\varphi_{beat,2a}(q,p) = \frac{2L}{\lambda} + \frac{c_0}{\lambda}\,\frac{p}{f_{AOM}} + \phi_q - \phi_{q+p} - \frac{\sigma}{2}\left(\left(\frac{2L}{c_0}\right)^2 + \frac{4L}{c_0}\,\frac{q+p}{f_{AOM}} + \frac{2qp+p^2}{f_{AOM}^2}\right) \tag{A.19}$$

If we define L' as in Chapter 2.3.3, we can write the beat frequencies as

$$f_{beat,2a}(q,p) = \frac{1}{T_R}\left(p + \frac{L}{L'}\right) \qquad \text{with} \quad L' = \frac{c_0}{2\,f_{AOM}}\ . \tag{A.20}$$

$$\begin{aligned}\varphi_{q+p}(t) - \varphi_q\left(t - \frac{2L}{c_0}\right) &= \frac{c_0}{\lambda}\left(t - \frac{q+p}{f_{AOM}}\right) + \frac{\sigma}{2}\left(t - \frac{q+p}{f_{AOM}}\right)^2 + \phi_{q+p} - \\ &\quad - \frac{c_0}{\lambda}\left(t - \frac{2L}{c_0} - \frac{q}{f_{AOM}}\right) - \frac{\sigma}{2}\left(t - \frac{2L}{c_0} - \frac{q}{f_{AOM}}\right)^2 - \phi_q \\ &= \frac{\sigma}{2}\left(\left(t^2 - 2\,\frac{q+p}{f_{AOM}}\,t + \frac{q^2+2qp+p^2}{f_{AOM}^2}\right) - \left(t^2 + \left(\frac{2L}{c_0}\right)^2 + \frac{q^2}{f_{AOM}^2}\right.\right. \\ &\quad \left.\left. - \frac{4L}{c_0}\,t - 2\,\frac{q}{f_{AOM}}\,t + \frac{4L}{c_0}\,\frac{q}{f_{AOM}}\right)\right) + \frac{2L}{\lambda} - \frac{c_0}{\lambda}\,\frac{p}{f_{AOM}} + \phi_{q+p} - \phi_q \\ &= \sigma\left(\frac{2L}{c_0} - \frac{p}{f_{AOM}}\right)t - \frac{\sigma}{2}\left(\left(\frac{2L}{c_0}\right)^2 + \frac{4L}{c_0}\,\frac{q}{f_{AOM}} - \frac{2qp+p^2}{f_{AOM}^2}\right) \\ &\quad + \frac{2L}{\lambda} - \frac{c_0}{\lambda}\,\frac{p}{f_{AOM}} + \phi_{q+p} - \phi_q \end{aligned} \tag{A.21}$$

The cosine is an even function, thus $\cos(-x) = \cos(x)$ holds, and we can also calculate $\varphi_q\left(t - \frac{2L}{c_0}\right) - \varphi_{q+p}(t)$.

$$\varphi_q\left(t - \frac{2L}{c_0}\right) - \varphi_{q+p}(t) = \sigma\left(\frac{p}{f_{AOM}} - \frac{2L}{c_0}\right)t + \frac{\sigma}{2}\left(\left(\frac{2L}{c_0}\right)^2 + \frac{4L}{c_0}\,\frac{q}{f_{AOM}} - \frac{2qp+p^2}{f_{AOM}^2}\right) - \frac{2L}{\lambda} + \frac{c_0}{\lambda}\,\frac{p}{f_{AOM}} + \phi_q - \phi_{q+p} \tag{A.22}$$

$$f_{beat,2b}(q,p) = \sigma\left(\frac{p}{f_{AOM}} - \frac{2L}{c_0}\right) = \frac{1}{T_R}\left(p - \frac{2\,f_{AOM}}{c_0}\,L\right) = \frac{1}{T_R}\left(p - \frac{L}{L'}\right) \tag{A.23}$$

$$\varphi_{beat,2b}(q,p) = \frac{\sigma}{2}\left(\left(\frac{2L}{c_0}\right)^2 + \frac{4L}{c_0}\,\frac{q+p}{f_{AOM}} - \frac{2qp+p^2}{f_{AOM}^2}\right) - \frac{2L}{\lambda} + \frac{c_0}{\lambda}\,\frac{p}{f_{AOM}} + \phi_q - \phi_{q+p} \tag{A.24}$$

A.1.1.3 Term $I_3(t)$

The third term is again an autocorrelation and thus similar to the first term.

$$\begin{aligned}
I_3(t) &= \eta^2\left|E\left(t - \frac{2L}{c_0}\right)\right|^2 = \eta^2\,\left(\sum_{q=1}^{N} E_q\left(t - \frac{2L}{c_0}\right)\,e^{i\,2\pi\varphi_q\left(t-\frac{2L}{c_0}\right)}\right)\cdot \\
&\qquad \cdot\left(\sum_{q=1}^{N} E_q\left(t - \frac{2L}{c_0}\right)\,e^{-i\,2\pi\varphi_q\left(t-\frac{2L}{c_0}\right)}\right) \\
&= \eta^2\sum_{p=0}^{N-1}\sum_{q=1}^{N-p}\frac{1}{2}\left(E_q\left(t - \frac{2L}{c_0}\right)\,E_{q+p}\left(t - \frac{2L}{c_0}\right)\,e^{i\,2\pi\left(\varphi_q\left(t-\frac{2L}{c_0}\right)-\varphi_{q+p}\left(t-\frac{2L}{c_0}\right)\right)}\right. \\
&\quad \left. + E_{q+p}\left(t - \frac{2L}{c_0}\right)\,E_q\left(t - \frac{2L}{c_0}\right)\,e^{i\,2\pi\left(\varphi_{q+p}\left(t-\frac{2L}{c_0}\right)-\varphi_q\left(t-\frac{2L}{c_0}\right)\right)}\right) \\
&= \eta^2\sum_{p=0}^{N-1}\sum_{q=1}^{N-p} E_q\left(t - \frac{2L}{c_0}\right)\,E_{q+p}\left(t - \frac{2L}{c_0}\right)\cdot \\
&\qquad \cdot\cos\left(2\pi\left(\varphi_q\left(t - \frac{2L}{c_0}\right) - \varphi_{q+p}\left(t - \frac{2L}{c_0}\right)\right)\right)
\end{aligned} \tag{A.25}$$

$$\begin{aligned}\varphi_q\left(t-\frac{2L}{c_0}\right)-\varphi_{q+p}\left(t-\frac{2L}{c_0}\right) &= \frac{c_0}{\lambda}\left(t-\frac{2L}{c_0}-\frac{q}{f_{AOM}}\right)+\frac{\sigma}{2}\left(t-\frac{2L}{c_0}-\frac{q}{f_{AOM}}\right)^2+\phi_q- \\ &\quad -\frac{c_0}{\lambda}\left(t-\frac{2L}{c_0}-\frac{q+p}{f_{AOM}}\right)-\frac{\sigma}{2}\left(t-\frac{2L}{c_0}-\frac{q+p}{f_{AOM}}\right)^2-\phi_{q+p} \\ &= \frac{\sigma}{2}\left(\left(t^2+\left(\frac{2L}{c_0}\right)^2+\frac{q^2}{f_{AOM}^2}-\frac{4L}{c_0}\,t-\frac{2\,q}{f_{AOM}}\,t\right.\right. \\ &\quad \left.-\frac{4L}{c_0}\,\frac{q}{f_{AOM}}\right)-\left(t^2+\left(\frac{2L}{c_0}\right)^2+\frac{q^2+2qp+p^2}{f_{AOM}^2}-\frac{4L}{c_0}\,t\right. \\ &\quad \left.\left.-\frac{q+p}{f_{AOM}}\,2t-\frac{4L}{c_0}\,\frac{q+p}{f_{AOM}}\right)\right)+\frac{c_0}{\lambda}\,\frac{p}{f_{AOM}}+\phi_q-\phi_{q+p} \\ &= \sigma\,\frac{p}{f_{AOM}}\,t-\frac{\sigma}{2}\left(\frac{p}{f_{AOM}}\,\frac{4L}{c_0}+\frac{2qp+p^2}{f_{AOM}^2}\right) \\ &\quad +\frac{c_0}{\lambda}\,\frac{p}{f_{AOM}}+\phi_q-\phi_{q+p} \end{aligned} \tag{A.26}$$

$$f_{beat,3}(q,p)=\sigma\,\frac{p}{f_{AOM}}=\frac{p}{T_R} \tag{A.27}$$

$$\varphi_{beat,3}(q,p)=\frac{c_0}{\lambda}\,\frac{p}{f_{AOM}}-\frac{\sigma}{2}\left(\frac{p}{f_{AOM}}\,\frac{4L}{c_0}+\frac{2qp+p^2}{f_{AOM}^2}\right)+\phi_q-\phi_{q+p} \tag{A.28}$$

A.1.2 Linear cavity

In the linear cavity, the light passes twice through the AOFS each round-trip. Therefore the chirp rate will be twice as big.

Chirp rate: $$\sigma=\frac{2\,f_{AOM}}{T_R} \tag{A.29}$$

Phase of mode q: $$\varphi_q(t)=\frac{c_0}{\lambda}\left(t-\frac{q}{2\,f_{AOM}}\right)+\frac{\sigma}{2}\left(t-\frac{q}{2\,f_{AOM}}\right)^2+\phi_q \tag{A.30}$$

Frequency of mode q: $$f_q(t)=\frac{d\varphi_q(t)}{dt}=\frac{c_0}{\lambda}+\sigma\left(t-\frac{q}{2\,f_{AOM}}\right) \tag{A.31}$$

Electric field: $$E(t)=\sum_{q=1}^{N}E_q(t)\;e^{i\,2\pi\varphi_q(t)} \qquad E_q(t)\in\Re \tag{A.32}$$

Intensity: $$I(t)=\frac{nc_0\epsilon_0}{2}\,|E(t)|^2 \tag{A.33}$$

The general description of the intensity after the Michelson interferometer is the same as for the ring cavity case.

$$I(t) \propto I_1(t) + I_2(t) + I_3(t) = \left| \delta\, E(t) + \eta\, E\left(t - \frac{2L}{c_0}\right) \right|^2$$
$$= \delta^2 |E(t)|^2 + \delta\eta \left(E^*(t)\ E\left(t - \frac{2L}{c_0}\right) + E(t)\ E^*\left(t - \frac{2L}{c_0}\right)\right) + \eta^2 \left| E\left(t - \frac{2L}{c_0}\right)\right|^2 \tag{A.34}$$

$$I_1(t) = \delta^2 |E(t)|^2 \tag{A.35}$$

$$I_2(t) = \delta\eta \left(E^*(t)\ E\left(t - \frac{2L}{c_0}\right) + E(t)\ E^*\left(t - \frac{2L}{c_0}\right)\right) \tag{A.36}$$

$$I_3(t) = \eta^2 \left| E\left(t - \frac{2L}{c_0}\right)\right|^2 \tag{A.37}$$

A.1.2.1 Term $I_1(t)$

The intensity calculation look the same as the ring cavity, too.

$$I_1(t) = \delta^2 |E(t)|^2 = \delta^2 \left(\sum_{q=1}^{N} E_q(t)\ e^{i\,2\pi\varphi_q(t)} \right) \left(\sum_{q=1}^{N} E_q(t)\ e^{-i\,2\pi\varphi_q(t)} \right)$$
$$= \delta^2 \sum_{p=0}^{N-1} \sum_{q=1}^{N-p} E_q(t)\ E_{q+p}(t)\ \cos\left(2\pi\left(\varphi_q(t) - \varphi_{q+p}(t)\right)\right) \tag{A.38}$$

But the phase term looks different from the ring cavity case.

$$\varphi_q(t) - \varphi_{q+p}(t) = \frac{c_0}{\lambda}\left(t - \frac{q}{2\,f_{AOM}}\right) + \frac{\sigma}{2}\left(t - \frac{q}{2\,f_{AOM}}\right)^2 + \phi_q$$
$$- \frac{c_0}{\lambda}\left(t - \frac{q+p}{2\,f_{AOM}}\right) - \frac{\sigma}{2}\left(t - \frac{q+p}{2\,f_{AOM}}\right)^2 - \phi_{q+p}$$
$$= \frac{\sigma}{2}\left(\left(t^2 - \frac{q}{f_{AOM}}\,t + \frac{q^2}{4\,f_{AOM}^2}\right) - \left(t^2 - \frac{q+p}{f_{AOM}}\,t + \frac{q^2+2qp+p^2}{4\,f_{AOM}^2}\right)\right)$$
$$+ \frac{c_0}{\lambda}\,\frac{p}{2\,f_{AOM}} + \phi_q - \phi_{q+p}$$
$$= \frac{\sigma}{2}\,\frac{p}{f_{AOM}}\,t - \frac{\sigma}{2}\,\frac{2qp+p^2}{4\,f_{AOM}^2} + \frac{c_0}{\lambda}\,\frac{p}{2\,f_{AOM}} + \phi_q - \phi_{q+p} \tag{A.39}$$

$$f_{beat,1}(q,p) = \frac{\sigma}{2}\,\frac{p}{f_{AOM}} = \frac{p}{T_R} \tag{A.40}$$

$$\varphi_{beat,1}(q,p) = \frac{c_0}{\lambda}\,\frac{p}{2\,f_{AOM}} - \frac{\sigma}{2}\,\frac{2qp+p^2}{4\,f_{AOM}^2} + \phi_q - \phi_{q+p} \tag{A.41}$$

A.1.2.2 Term $I_2(t)$

$$
\begin{aligned}
I_2(t) &= \delta\eta \left(E^*(t)\ E\left(t - \frac{2L}{c_0}\right) + E(t)\ E^*\left(t - \frac{2L}{c_0}\right)\right) \\
&= \delta\eta \sum_{p=0}^{N-1} \sum_{q=1}^{N-p} E_q(t)\ E_{q+p}\left(t - \frac{2L}{c_0}\right) \cos\left(2\pi\left(\varphi_q(t) - \varphi_{q+p}\left(t - \frac{2L}{c_0}\right)\right)\right) \\
&\quad + \sum_{p=0}^{N-1} \sum_{q=1}^{N-p} E_{q+p}(t)\ E_q\left(t - \frac{2L}{c_0}\right) \cos\left(2\pi\left(\varphi_{q+p}(t) - \varphi_q\left(t - \frac{2L}{c_0}\right)\right)\right) \qquad \text{(A.42)}
\end{aligned}
$$

This term can be decomposed into two cosines. The difference to the ring cavity case is again only apparent in the phase terms.

$$
\begin{aligned}
\varphi_q(t) - \varphi_{q+p}\left(t - \frac{2L}{c_0}\right) &= \frac{c_0}{\lambda}\left(t - \frac{q}{2\,f_{AOM}}\right) + \frac{\sigma}{2}\left(t - \frac{q}{2\,f_{AOM}}\right)^2 + \phi_q \\
&\quad - \frac{c_0}{\lambda}\left(t - \frac{2L}{c_0} - \frac{q+p}{2\,f_{AOM}}\right) - \frac{\sigma}{2}\left(t - \frac{2L}{c_0} - \frac{q+p}{2\,f_{AOM}}\right)^2 - \phi_{q+p} \\
&= \frac{\sigma}{2}\left(\left(t^2 - \frac{q}{f_{AOM}}\,t + \frac{q^2}{4\,f_{AOM}^2}\right) - \left(t^2 + \left(\frac{2L}{c_0}\right)^2\right.\right. \\
&\quad \left.\left. + \frac{q^2+2qp+p^2}{4\,f_{AOM}^2} + \frac{4L}{c_0}\,\frac{q+p}{2\,f_{AOM}} - \frac{q+p}{f_{AOM}}\,t - \frac{4L}{c_0}\,t\right)\right) \\
&\quad + \frac{2L}{\lambda} + \frac{c_0}{\lambda}\,\frac{p}{2\,f_{AOM}} + \phi_q - \phi_{q+p} \\
&= \frac{\sigma}{2}\left(\frac{p}{f_{AOM}} + \frac{4L}{c_0}\right)t - \frac{\sigma}{2}\left(\left(\frac{2L}{c_0}\right)^2 + \frac{2L}{c_0}\,\frac{q+p}{f_{AOM}} + \frac{2qp+p^2}{4\,f_{AOM}^2}\right) \\
&\quad + \frac{2L}{\lambda} + \frac{c_0}{\lambda}\,\frac{p}{2\,f_{AOM}} + \phi_q - \phi_{q+p} \qquad \text{(A.43)}
\end{aligned}
$$

$$
f_{beat,2a}(q,p) = \frac{\sigma}{2}\left(\frac{p}{f_{AOM}} + \frac{4L}{c_0}\right) = \frac{1}{T_R}\left(p + \frac{4\,f_{AOM}}{c_0}\,L\right) \qquad \text{(A.44)}
$$

$$
\varphi_{beat,2a}(q,p) = \frac{2L}{\lambda} + \frac{c_0}{\lambda}\,\frac{p}{2\,f_{AOM}} + \phi_q - \phi_{q+p} - \frac{\sigma}{2}\left(\left(\frac{2L}{c_0}\right)^2 + \frac{2L}{c_0}\,\frac{q+p}{f_{AOM}} + \frac{2qp+p^2}{4\,f_{AOM}^2}\right) \qquad \text{(A.45)}
$$

If we define again L', we can write the beat frequencies as

$$
f_{beat,2a}(q,p) = \frac{1}{T_R}\left(p + \frac{L}{L'}\right) \qquad \text{where} \quad L' = \frac{c_0}{4\,f_{AOM}}\ . \qquad \text{(A.46)}
$$

$$\begin{aligned}\varphi_{q+p}(t) - \varphi_q\left(t - \frac{2L}{c_0}\right) &= \frac{c_0}{\lambda}\left(t - \frac{q+p}{2\,f_{AOM}}\right) + \frac{\sigma}{2}\left(t - \frac{q+p}{2\,f_{AOM}}\right)^2 + \phi_{q+p} - \\ &\quad - \frac{c_0}{\lambda}\left(t - \frac{2L}{c_0} - \frac{q}{2\,f_{AOM}}\right) - \frac{\sigma}{2}\left(t - \frac{2L}{c_0} - \frac{q}{2\,f_{AOM}}\right)^2 - \phi_q \\ &= \frac{\sigma}{2}\left(\left(t^2 - \frac{q+p}{f_{AOM}}\,t + \frac{q^2+2qp+p^2}{4\,f_{AOM}^2}\right) - \left(t^2 + \left(\frac{2L}{c_0}\right)^2\right.\right. \\ &\quad \left.\left. + \frac{q^2}{4\,f_{AOM}^2} - \frac{4L}{c_0}\,t - \frac{q}{f_{AOM}}\,t + \frac{2L}{c_0}\,\frac{q}{f_{AOM}}\right)\right) \\ &\quad + \frac{2L}{\lambda} - \frac{c_0}{\lambda}\,\frac{p}{2\,f_{AOM}} + \phi_{q+p} - \phi_q \\ &= \frac{\sigma}{2}\left(\frac{4L}{c_0} - \frac{p}{f_{AOM}}\right)t - \frac{\sigma}{2}\left(\left(\frac{2L}{c_0}\right)^2 + \frac{2L}{c_0}\,\frac{q}{f_{AOM}} - \frac{2qp+p^2}{4\,f_{AOM}^2}\right) \\ &\quad + \frac{2L}{\lambda} - \frac{c_0}{\lambda}\,\frac{p}{2\,f_{AOM}} + \phi_{q+p} - \phi_q \end{aligned} \tag{A.47}$$

Again, we change the sign and so we get

$$\begin{aligned}\varphi_q\left(t - \frac{2L}{c_0}\right) - \varphi_{q+p}(t) &= \frac{\sigma}{2}\left(\frac{p}{f_{AOM}} - \frac{4L}{c_0}\right)t + \frac{\sigma}{2}\left(\left(\frac{2L}{c_0}\right)^2 + \frac{2L}{c_0}\,\frac{q}{f_{AOM}} - \frac{2qp+p^2}{4\,f_{AOM}^2}\right) \\ &\quad - \frac{2L}{\lambda} + \frac{c_0}{\lambda}\,\frac{p}{2\,f_{AOM}} + \phi_q - \phi_{q+p} \end{aligned} \tag{A.48}$$

$$f_{beat,2b}(q,p) = \frac{\sigma}{2}\left(\frac{p}{f_{AOM}} - \frac{4L}{c_0}\right) = \frac{1}{T_R}\left(p - \frac{4\,f_{AOM}}{c_0}\,L\right) = \frac{1}{T_R}\left(p - \frac{L}{L'}\right) \tag{A.49}$$

$$\varphi_{beat,2b}(q,p) = \frac{\sigma}{2}\left(\left(\frac{2L}{c_0}\right)^2 + \frac{2L}{c_0}\,\frac{q+p}{f_{AOM}} - \frac{2qp+p^2}{4\,f_{AOM}^2}\right) - \frac{2L}{\lambda} + \frac{c_0}{\lambda}\,\frac{p}{2\,f_{AOM}} + \phi_q - \phi_{q+p} \tag{A.50}$$

A.1.2.3 Term $I_3(t)$

$$\begin{aligned} I_3(t) = \eta^2\left|E\left(t - \frac{2L}{c_0}\right)\right|^2 &= \eta^2\,\left(\sum_{q=1}^{N} E_q\left(t - \frac{2L}{c_0}\right)\,e^{i\,2\pi\varphi_q\left(t - \frac{2L}{c_0}\right)}\right)\cdot \\ &\quad \cdot\left(\sum_{q=1}^{N} E_q\left(t - \frac{2L}{c_0}\right)\,e^{-i\,2\pi\varphi_q\left(t - \frac{2L}{c_0}\right)}\right) \\ &= \eta^2\sum_{p=0}^{N-1}\,\sum_{q=1}^{N-p} E_q\left(t - \frac{2L}{c_0}\right)\,E_{q+p}\left(t - \frac{2L}{c_0}\right)\cdot \\ &\quad \cdot\cos\left(2\pi\left(\varphi_q\left(t - \frac{2L}{c_0}\right) - \varphi_{q+p}\left(t - \frac{2L}{c_0}\right)\right)\right) \end{aligned} \tag{A.51}$$

$$\begin{aligned}
\varphi_q\left(t-\frac{2L}{c_0}\right)-\varphi_{q+p}\left(t-\frac{2L}{c_0}\right) &= \frac{c_0}{\lambda}\left(t-\frac{2L}{c_0}-\frac{q}{2\,f_{AOM}}\right)+\frac{\sigma}{2}\left(t-\frac{2L}{c_0}-\frac{q}{2\,f_{AOM}}\right)^2 \\
&\quad -\frac{c_0}{\lambda}\left(t-\frac{2L}{c_0}-\frac{q+p}{2\,f_{AOM}}\right)-\frac{\sigma}{2}\left(t-\frac{2L}{c_0}-\frac{q+p}{2\,f_{AOM}}\right)^2 \\
&\quad +\phi_q-\phi_{q+p} \\
&= \frac{\sigma}{2}\left(\left(t^2+\left(\frac{2L}{c_0}\right)^2+\frac{q^2}{4\,f_{AOM}^2}-\frac{4L}{c_0}\,t-\frac{q}{f_{AOM}}\,t\right.\right. \\
&\quad \left.-\frac{2L}{c_0}\,\frac{q}{f_{AOM}}\right)-\left(t^2+\left(\frac{2L}{c_0}\right)^2+\frac{q^2+2qp+p^2}{4\,f_{AOM}^2}-\frac{4L}{c_0}\,t\right. \\
&\quad \left.\left.-\frac{q+p}{f_{AOM}}\,t-\frac{2L}{c_0}\,\frac{q+p}{f_{AOM}}\right)\right)+\frac{c_0}{\lambda}\,\frac{p}{2\,f_{AOM}}+\phi_q-\phi_{q+p} \\
&= \frac{\sigma}{2}\,\frac{p}{f_{AOM}}\,t-\frac{\sigma}{2}\left(\frac{p}{f_{AOM}}\,\frac{2L}{c_0}+\frac{2qp+p^2}{4\,f_{AOM}^2}\right) \\
&\quad +\frac{c_0}{\lambda}\,\frac{p}{2\,f_{AOM}}+\phi_q-\phi_{q+p} \qquad \text{(A.52)}
\end{aligned}$$

$$f_{beat,3}(q,p)=\frac{\sigma}{2}\,\frac{p}{f_{AOM}}=\frac{p}{T_R} \qquad \text{(A.53)}$$

$$\varphi_{beat,3}(q,p)=\frac{c_0}{\lambda}\,\frac{p}{2\,f_{AOM}}-\frac{\sigma}{2}\left(\frac{p}{f_{AOM}}\,\frac{2L}{c_0}+\frac{2qp+p^2}{4\,f_{AOM}^2}\right)+\phi_q-\phi_{q+p} \qquad \text{(A.54)}$$

A.2 Laser stability simulations

In [24], Siegman explains the ABCD formalism in ray optics. The basic idea is to assign a matrix to every part that the light ray passes. We do not want to go into detail of the theory. In the following only the most important results are described. In order to

Distance d in Air	$\begin{pmatrix} 1 & d \\ 0 & 1 \end{pmatrix}$
Distance d in Medium n	$\begin{pmatrix} 1 & \frac{d}{n} \\ 0 & 1 \end{pmatrix}$
Lens (Curved Mirror) with Focal Length f	$\begin{pmatrix} 1 & 0 \\ -\frac{1}{f} & 1 \end{pmatrix}$

Table A.2.: ABCD Matrices of Various Optical Elements

calculate the ABCD matrix of a sequence of optical elements, one must only multiply the matrices. There is also a stability condition. It states that the absolute value of the trace must be smaller than 2. That can be written as

$$-1 < \frac{1}{2}(A+D) < 1 \qquad \text{with the ABCD matrix} \begin{pmatrix} A & B \\ C & D \end{pmatrix} . \tag{A.55}$$

In order to calculate the stability of a laser cavity, one only needs to multiply all corresponding ABCD matrices for one round-trip and check if the condition is fulfilled.

A.2.1 Laser stability with one parameter

The stability check was implemented in Matlab and the following shows the source code.

```
clear all;
close all;
% define range and step size of the unknown
x = 22:0.001:27;
% create array for stability
y = zeros(size(x));

for i=1:length(x)
    % define focal lengths and refractive indices
    f_Cry = 25;
    f_AOM = 200;
    n_Cry = 1.76;
    n_AOM = 2.3;

    % assign value for the unknown
    Cm1Cry = x(i);
```

```
    % define length values
    Cry = 2.9;
    CryCm2 = 24.3;
    Cm2Cm3 = 1357;
    Cm3AOM = 200;
    AOM = 30;
    AOMCm4 = 200;
    Cm4Cm1 = 2030;

    % multiply matrices
    erg = [1 0; -1/f_Cry 1] * [1 Cm1Cry; 0 1];
    erg = erg * [1 Cry/n_Cry; 0 1];
    erg = erg * [1 CryCm2; 0 1];
    erg = erg * [1 0; -1/f_Cry 1];
    erg = erg * [1 Cm2Cm3; 0 1];
    erg = erg * [1 0; -1/f_AOM 1];
    erg = erg * [1 Cm3AOM; 0 1];
    erg = erg * [1 AOM/n_AOM; 0 1];
    erg = erg * [1 AOMCm4; 0 1];
    erg = erg * [1 0; -1/f_AOM 1];
    erg = erg * [1 Cm4Cm1; 0 1];

    % calculate half of the trace
    stab = 1/2 * (erg(1,1) + erg(2,2));
    % squaring makes comparison easier
    stab = stab^2;

    % check stability
    if (stab < 1)
        y(i) = 1 - stab;
    else
        y(i) = 0;
    end

end

% graphical output
plot(x, y, 'b', 'LineWidth', 3);
xlabel('CM1 - Crystal / mm', 'FontSize', 16);
ylabel('Stability', 'FontSize', 16);
set(gcf, 'units', 'normalized', 'outerposition', [0 0.03 1 0.97]);
```

A.2.2 Laser stability zones

The source to get a two-dimensional plot for the stability zones is an extention of the previous source code.

```
clear all;
close all;
% define range and step size of the unknowns
x = 20:0.01:30;
y = 180:0.1:280;
% create array for stability
z = zeros(length(x), length(y));

for i=1:length(x)
    for j=1:length(y)
        % define focal lengths and refractive indices
        f_Cry = 25;
        f_AOM = 200;
        n_Cry = 1.76;
        n_AOM = 2.3;

        % define length values
        Cm1Cry = x(i); % assign value for the first unknown
        Cry = 2.9;
        CryCm2 = 24.3;
        Cm2Cm3 = 1357;
        Cm3AOM = y(j); % assign value for the second unknown
        AOM = 30;
        AOMCm4 = 200;
        Cm4Cm1 = 2030;

        % multiply matrices
        erg = [1 0; -1/f_Cry 1] * [1 Cm1Cry; 0 1];
        erg = erg * [1 Cry/n_Cry; 0 1];
        erg = erg * [1 CryCm2; 0 1];
        erg = erg * [1 0; -1/f_Cry 1];
        erg = erg * [1 Cm2Cm3; 0 1];
        erg = erg * [1 0; -1/f_AOM 1];
        erg = erg * [1 Cm3AOM; 0 1];
        erg = erg * [1 AOM/n_AOM; 0 1];
        erg = erg * [1 AOMCm4; 0 1];
        erg = erg * [1 0; -1/f_AOM 1];
        erg = erg * [1 Cm4Cm1; 0 1];

        % calculate half of the trace
        stab = 1/2 * (erg(1,1) + erg(2,2));
        % squaring makes comparison easier
        stab = stab^2;
```

```
        % check stability
        if (stab < 1)
            z(i, j) = 1 - stab;
        else
            z(i, j) = 0;
        end
    end
end

% graphical output
surf(x, y, z', 'EdgeColor', 'none', 'FaceColor', 'interp', 'FaceLighting', 'phong');
set(gcf, 'units', 'normalized', 'outerposition', [0 0.03 1 0.97]);
view([0 90]);
xlabel('CM1 - Crystal / mm', 'FontSize', 16);
ylabel('CM3 - AOM / mm', 'FontSize', 16);
zlabel('Stability', 'FontSize', 16);
```

Bibliography

[1] Y. Oike, M. Ikeda, A. Asada, "Design and Implementation of Real-Time 3-D Image Sensor With 640 480 Pixel Resolution", *IEEE Journal of Solid-State Circuits*, Volume 39, pp. 622-628 (2004)

[2] A. Nemecek, K. Oberhauser, H. Zimmermann "Distance Measurement Sensor With PIN-Photodiode and Bridge Circuit", *IEEE Sensors Journal*, Volume 6, pp. 391-397 (2006)

[3] G. Zach, H. Zimmermann, "A 2x32 Range-Finding Sensor Array with Pixel-Inherent Suppression of Ambient Light up to 120klx", *IEEE ISSCC*, (2009), pp. 352–353

[4] G. Zach, M. Davidovic, H. Zimmermann, "Extraneous-light resistant multipixel range sensor based on a low-power correlating pixel-circuit", *IEEE ESSCIRC*, pp. 236-239 (2009)

[5] C.C. Liebe, S. Dubovitsky, R. Peters, "3D Metrology Camera", *IEEE Aerospace Conference*, pp. 1-8 (2007)

[6] I. Coddington, W. C. Swann, L. Nenadovic, N. R. Newbury, "Rapid and precise absolute distance measurements at long range", *Nature Photonics*, Volume 3, pp. 351-356 (2009)

[7] P.D. Hale, F.V. Kowalski, "Output Characterization of a Frequency Shifted Feedback Laser: Theory and Experiment", *IEEE Journal of Quantum Electronics*, Volume 26, pp. 1845-1851 (1990)

[8] I.C.M. Littler, J.H. Eschner, "The cw modeless laser: model calculations of an active frequency shifted feedback cavity", *Optics Communications*, Volume 87, pp. 44-52 (1992)

[9] I.C.M. Littler, S. Balle, K. Bergmann, "The cw modeless laser: spectral control, performance data and build-up dynamics", *Optics Communications*, Volume 88, pp. 514-522 (1992)

[10] G. Bonnet, S. Balle, T. Kraft, K. Bergmann, "Dynamics and self-modelocking of a titanium-sapphire laser with intracavity frequency shifted feedback", *Optics Communications*, Volume 123, pp. 790-800 (1996)

[11] M. Stellpflug, G. Bonnet, B.W. Shore, K. Bergmann, "Dynamics of frequency shifted feedback lasers: simulation studies", *Optics Express*, Volume 11, pp.2060-2080 (2003)

[12] Koichiro Nakamura, Fumitoshi Abe, Kumio Kasahara, Takefumi Hara, Manabu Sato, Hiromasa Ito, "Spectral Characteristics of an All Solid-state Frequency-Shifted Feedback Laser", *IEEE JOURNAL OF QUANTUM ELECTRONICS*, Volume 33, pp. 103-111 (1997)

[13] K. Nakamura, T. Miyahara, H. Ito, "Observation of a highly phase-correlated chirped frequency comb output from a frequency-shifted feedback laser", Applied Physics Letters, Volume 72, pp. 2631-2633 (1998)

[14] K. Nakamura, T. Miyahara, M. Yoshida, T. Hara, H, Ito, "A New Technique of Optical Ranging by a Frequency-Shifted Feedback Laser", *IEEE Photonics Technology Letters*, Volume 10, pp. 1772-1774 (1998)

[15] K. Nakamura, T. Hara, M. Yoshida, Toshiharu Miyahara, Hiromasa Ito, "Optical Frequency Domain Ranging by a Frequency-Shifted Feedback Laser", *IEEE Journal of Quantum Electronics*, Volume 36, pp. 305-316 (2000)

[16] L.P. Yatsenko, B.W. Shore, K. Bergmann, "Coherence in the output spectrum of frequency shifted feedback lasers", *Optics Communications*, Volume 282, pp. 300-309 (2009)

[17] L.P. Yatsenko, B.W. Shore, K. Bergmann, "Theory of a frequency-shifted feedback laser", *Optics Communications*, Volume 236, pp. 183-202 (2004)

[18] L.P. Yatsenko, B.W. Shore, K. Bergmann, "Ranging and interferometry with a frequency shifted feedback laser", *Optics Communications*, Volume 242, pp. 581-598 (2004)

[19] V.V. Ogurtsov, L.P. Yatsenko, V.M. Khodakovskyy, B.W. Shore, G. Bonnet, K. Bergmann, "High accuracy ranging with Yb^{3+}-doped fiber-ring frequency-shifted feedback laser with phase-modulated seed", *Optics Communications*, Volume 266, pp. 266-273 (2006)

[20] V.V. Ogurtsov, L.P. Yatsenko, V.M. Khodakovskyy, B.W. Shore, G. Bonnet, K. Bergmann, "Experimental characterization of an Yb^{3+}-doped fiber ring laser with frequency-shifted feedback", *Optics Communications*, Volume 266, pp. 627-637 (2006)

[21] V.V. Ogurtsov, V.M. Khodakovskyy, L.P. Yatsenko, B.W. Shore, G. Bonnet, K. Bergmann, "An all-fiber frequency-shifted feedback laser for optical ranging; signal variation with distance", *Optics Communications*, Volume 281, pp. 1679-1685 (2008)

[22] L.P. Yatsenko, B.W. Shore, K. Bergmann, "An intuitive picture of the physics underlying optical ranging using frequency shifted feedback lasers seeded by a phase-modulated field", *Optics Communications*, Volume 282, pp. 2212-2216 (2009)

[23] Bertram A. Auld: *Acoustic Fields and Waves in Solids, Vol. 1*, Interscience, 1973. - ISBN 0471037001

[24] Anthony E. Siegman: *Lasers*, University Science Books, 1986. - ISBN 0935702113

Acknowledgments

I would like to thank the people involved in this project for their support.

- **Andrius Baltuška** for giving me the opportunity to build the laser with his group's equipment, and for the support by him and his team.

- **Alma Fernández González** for providing the 3mm Ti:Sa crystal from her stock.

- **Oliver Mücke** for introducing me in building lasers, for support in the theoretical model as well as building the laser, for his guidance in the scientific work, and for his feedback in writing this thesis.

- **Audrius Pugzlys** for his help and support in building the laser.

- **Robert Swoboda** for his support with the equipment that was needed to build the laser and to do the measurement.

- **Horst Zimmermann** for giving me the opportunity to work at this topic and for his trust and support during the construction of the laser.

- **Family and friends** for their support.